International Journal of Coal Geology 206 (2019) 46–64

Contents lists available at ScienceDirect

International Journal of Coal Geology

journal homepage: www.elsevier.com/locate/coal

Understanding organic matter heterogeneity and maturation rate by Raman spectroscopy

Seyedalireza Khatibi[a,*], Mehdi Ostadhassan[a,*], Paul Hackley[b], David Tuschel[c], Arash Abarghani[a], Bailey Bubach[a]

[a] University of North Dakota, Grand Forks, ND, USA
[b] U.S. Geological Survey, Reston, VA, USA
[c] HORIBA Scientific, 3880 Park Avenue, Edison, NJ, USA

ARTICLE INFO

Keywords:
Organic matter
Heterogeneity
Raman spectroscopy
Maturation rate
Hydrous pyrolysis

ABSTRACT

Solid organic matter (OM) in sedimentary rocks produces petroleum and solid bitumen when it undergoes thermal maturation. The solid OM is a 'geomacromolecule', usually representing a mixture of various organisms with distinct biogenic origins, and can have high heterogeneity in composition. Programmed pyrolysis is a common method to reveal bulk geochemical characteristics of the dominant OM, while detailed organic petrography is required to reveal information about the biogenic origin of contributing macerals. Despite the advantages of programmed pyrolysis, it cannot provide information about the heterogeneity of chemical compositions present in the individual OM types. Therefore, other analytical techniques such as Raman spectroscopy are necessary.

In this study, we compared geochemical characteristics and Raman spectra of two sets of naturally and artificially matured Bakken source rock samples. A continuous Raman spectral map on solid bitumen particles was created from the artificially matured hydrous pyrolysis residues, in particular, to show the systematic chemical modifications in microscale. Spectroscopic data was plotted for both sets against thermal maturity to compare maturation rate/path for these two separate groups. The outcome showed that artificial maturation through hydrous pyrolysis does not follow the same trend as naturally-matured samples although having similar solid bitumen reflectance values (%SBRo).

Furthermore, Raman spectroscopy of solid bitumen from artificially matured samples indicated the heterogeneity of OM decreases as maturity increases. This may represent an alteration in chemical structure towards more uniform compounds at higher maturity. This study may emphasize the necessity of using analytical methods such as Raman spectroscopy along with conventional geochemical methods to better reveal the underlying chemical structure of OM. Finally, observation by Raman spectroscopy of chemical alteration of OM during artificial maturation may assist in the proposal of improved pyrolysis protocols to better resemble natural geologic processes.

1. Introduction

Shale is the most abundant fine-grained sedimentary rock and is formed from compaction of silt and clay-sized minerals which also may contain a significant amount of solid organic matter (OM). Kerogen (the insoluble portion of OM) is a macromolecule and a mixture of OM types with different origins (Types I, II, III and IV) (Garcette-Lepecq et al., 2000; Ostadhassan et al., 2018). When kerogen experiences maturation, weight concentration and the composition of the individual macerals evolve (Yang et al., 2017). During this process, bigger molecules will break down and the outcome will be hydrocarbons and bitumen in addition to water, CO_2 etc. (Schito et al., 2017). The remainder of the organic matter acts as the storage reservoir by developing nanoscale pores which hold generated hydrocarbons (Curtis et al., 2012; Chen and Xiao, 2014). Furthermore, the process of thermal maturation will cause or enhance the development of local heterogeneities within the remaining organic matter (Kong et al., 2018). This is due to differences in the rate of maturation for the existing kerogen based on differences in type and origin (Yang et al., 2017). Additionally, heterogeneity may also be due to local variations in thermal alteration that is imposed on the organic matter by catalysis from nearby mineral grains (Pan et al., 2009). Understanding these heterogeneous patterns will enable better

* Corresponding authors.
E-mail addresses: Seyedalireza.khatibi@und.edu (S. Khatibi), mehdi.ostadhassan@und.edu (M. Ostadhassan).

https://doi.org/10.1016/j.coal.2019.03.009
Received 16 October 2018; Received in revised form 14 March 2019
Available online 17 March 2019
0166-5162/

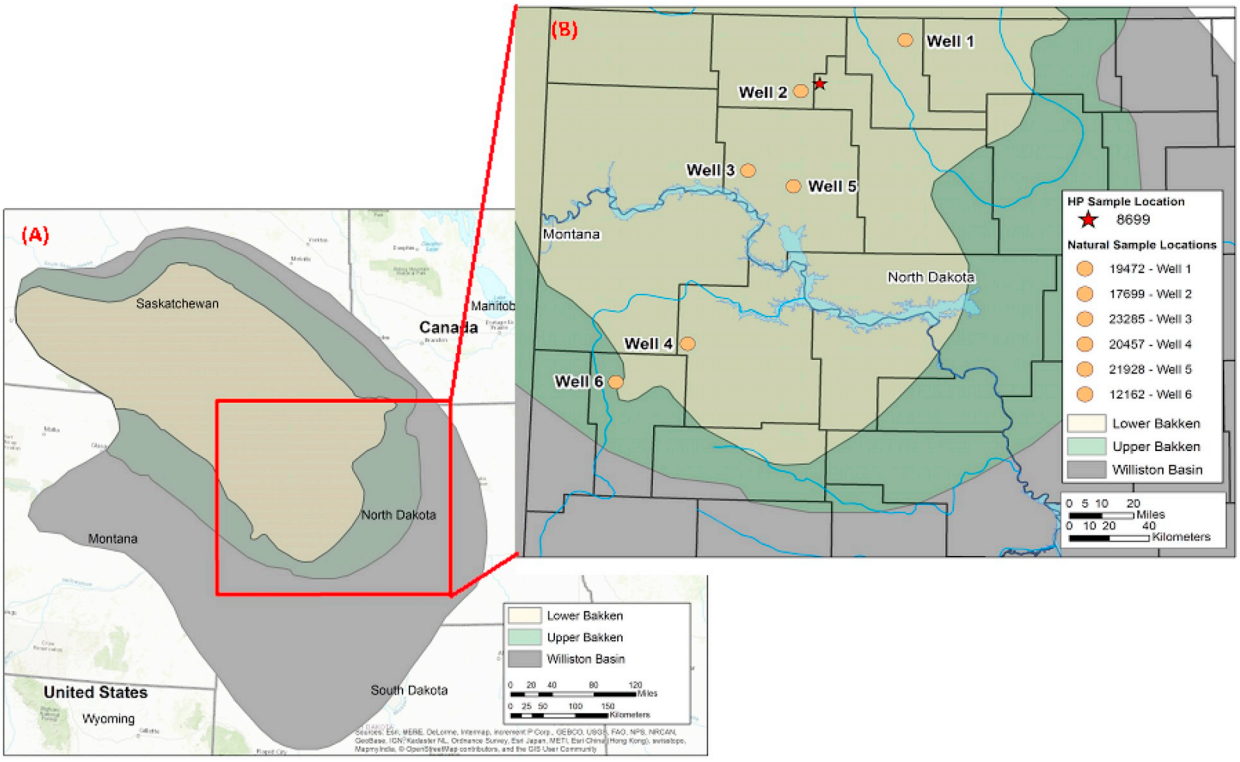

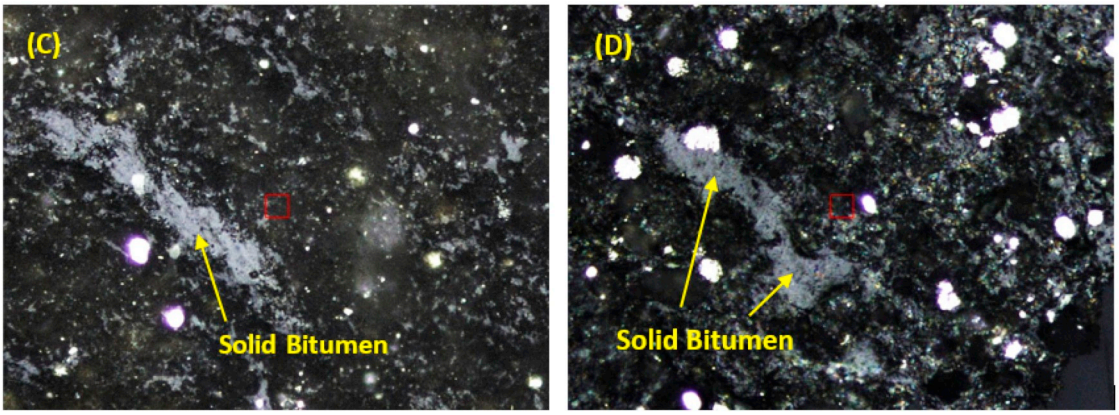

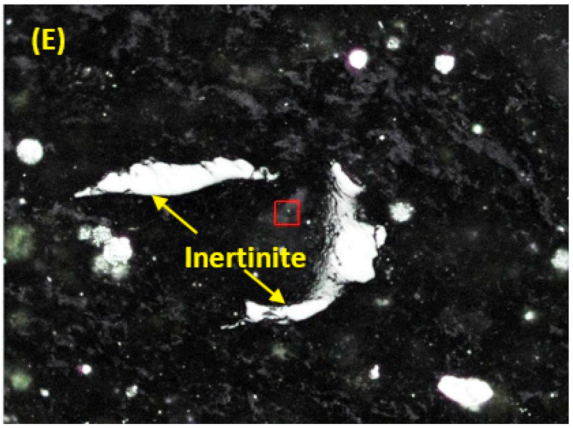

Fig. 1. (A) and (B) location of the Bakken formation and the wells used in this study for sampling; (C) and (D) Solid bitumen in samples of Well 1 and Well 5, respectively, (E) occurrence of dispersed organic matter in the form of inertinite in Well 4. The red square in the middle of each image is a scale of 5 μm of each side. (For interpretation of the references to colour in this figure legend, the reader is referred to the web version of this article.)

Table 1
Geochemical properties of two sets of data. Note the systematic changes in Tmax, TOC, S2, HI, and PI with increasing maturity in both naturally and artificialy matured samples.

	Sample No.	Depth (ft)	TOC (wt%)	S1 (mg HC/g)	S2 (mg HC/g)	T_{max} (^{0})	HI (S2*100/ TOC)	OI (S3*100/ TOC)	PI S1/(S1 + S2)	SBRo (%)	HP time (hrs.)	HP temp. (^{0}c)
Artificially matured sample by HP	HP1	7652	14.59	8.28	80.83	428	554	8	0.09	0.32	72	original
	HP2		13.3	4.5	72.02	429	542	10	0.06	0.35	72	280
	HP3		15.15	8	87.1	434	575	7	0.08	0.38	72	300
	HP4		11.55	7.85	72.68	436	629	12	0.1	0.49	72	310
	HP5		10.66	6.78	53.47	431	502	9	0.11	0.54	72	320
	HP6		7.39	4.18	18.47	442	250	11	0.18	0.95	72	340
	HP7		8.12	3.19	11.16	451	137	12	0.22	1.19	72	350
	HP8		7.95	3.97	8.07	462	102	6	0.33	1.29	72	360
In situ matured samples	Well 1	5438	24.71	7.97	128.71	419	520	8	0.06	0.38	–	–
	Well 2	8326	16.27	8.27	90.69	428	557	2	0.08	0.54	–	–
	Well 3	9886	15.76	9.27	83.7	432	531	1	0.1	0.59	–	–
	Well 4	10,555	13.26	0.31	33.01	449	260	1	0.013	0.86	–	–
	Well 5	10,725.5	9.04	6.13	13.94	450	154	1	0.31	0.94	–	–
	Well 6	11,199	16.36	0.71	28.05	452	171	1	0.024	0.92	–	–

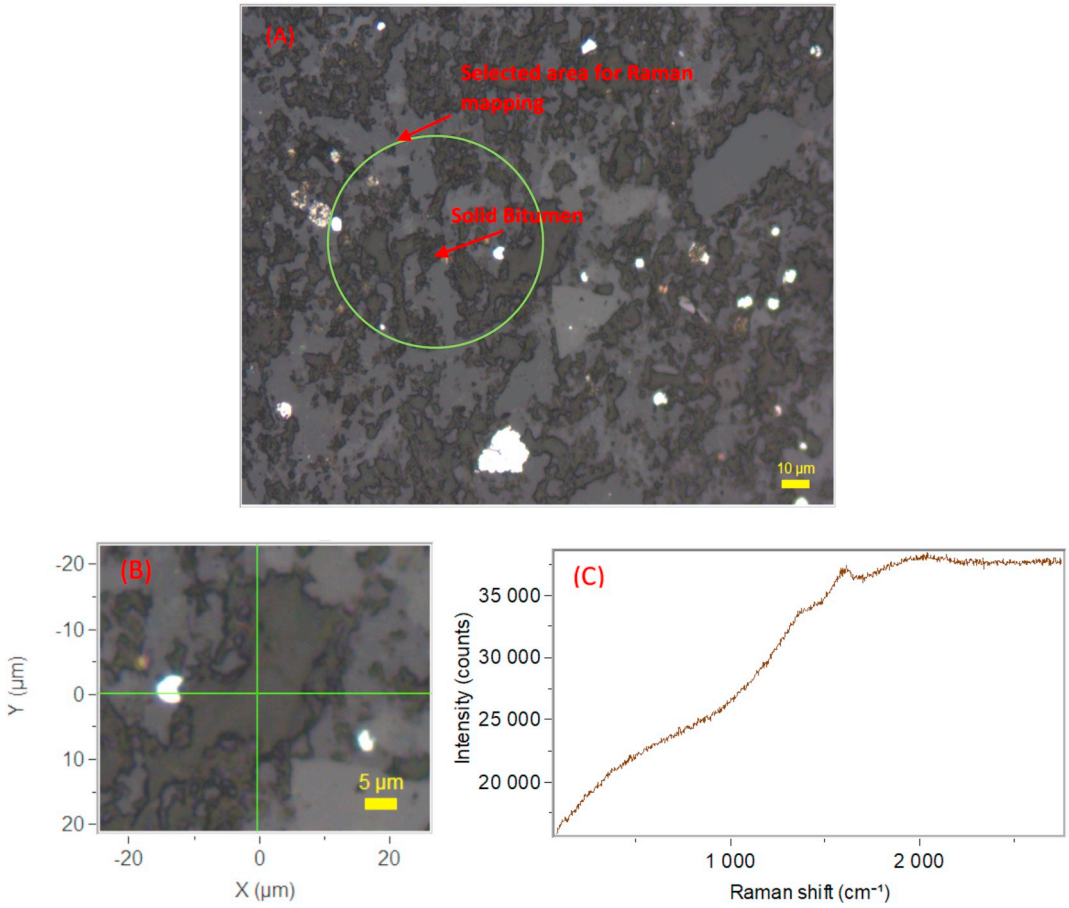

Fig. 2. (A) area selected for Raman spectroscopy, a complete spectrum is acquired at every pixel of the area of interest (1000 spectra are acquired which can all be processed with the same processing steps), (B) a point selected on solid bitumen, (C) and its corresponding Raman spectrum.

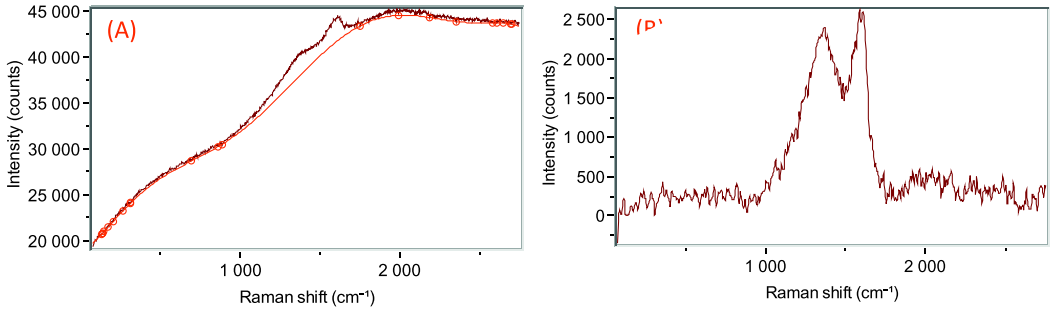

Fig. 3. Raman signals before (A) and after (B) baseline correction for Well 2 as a naturally matured sample.

characterization of geochemical, petrophysical and geomechanical properties of organic matter from a molecular point of view (Curtis et al., 2012). In addition, these studies will enhance our understanding of mechanisms related to generation and migration of hydrocarbons, especially in self-sourced unconventional reservoirs.

Despite the importance of assessing shale OM heterogeneity, common bulk-rock geochemical measurement methods that have been utilized for decades such as programmed pyrolysis and LECO total organic carbon (TOC) are incapable of providing information specific to individual OM types. SEM (scanning electron microscope) analysis combined with energy-dispersive X-ray spectroscopy (SEM-EDS) can detect local changes in the abundance of higher atomic weight elements. However, it cannot recognize variations in molecular chemical components which are the driving force behind OM heterogeneity (Schumacher et al., 2005; Piani et al., 2012). Organic petrography allows identification of various types of organic components but cannot detect molecular compositions (Hackley and Cardott, 2016). Moreover, geochemistry of organic matter which is controlled by molecular compounds is usually investigated by pyrolysis which is artificially maturing the samples. Yet, to obtain meaningful results, many parameters (pyrogram) that are involved in the experiments should be set accurately to resemble a natural maturation path (Carvajal-Ortiz and Gentzis, 2015). This process can be done in the absence or presence of water, anhydrous pyrolysis (AHP) and hydrous pyrolysis (HP), respectively.

Lewan et al. (1979, b) discussed and performed several experiments on the role of water in petroleum formation. He showed that AHP will result in higher organic maturation rate compared to HP at the same

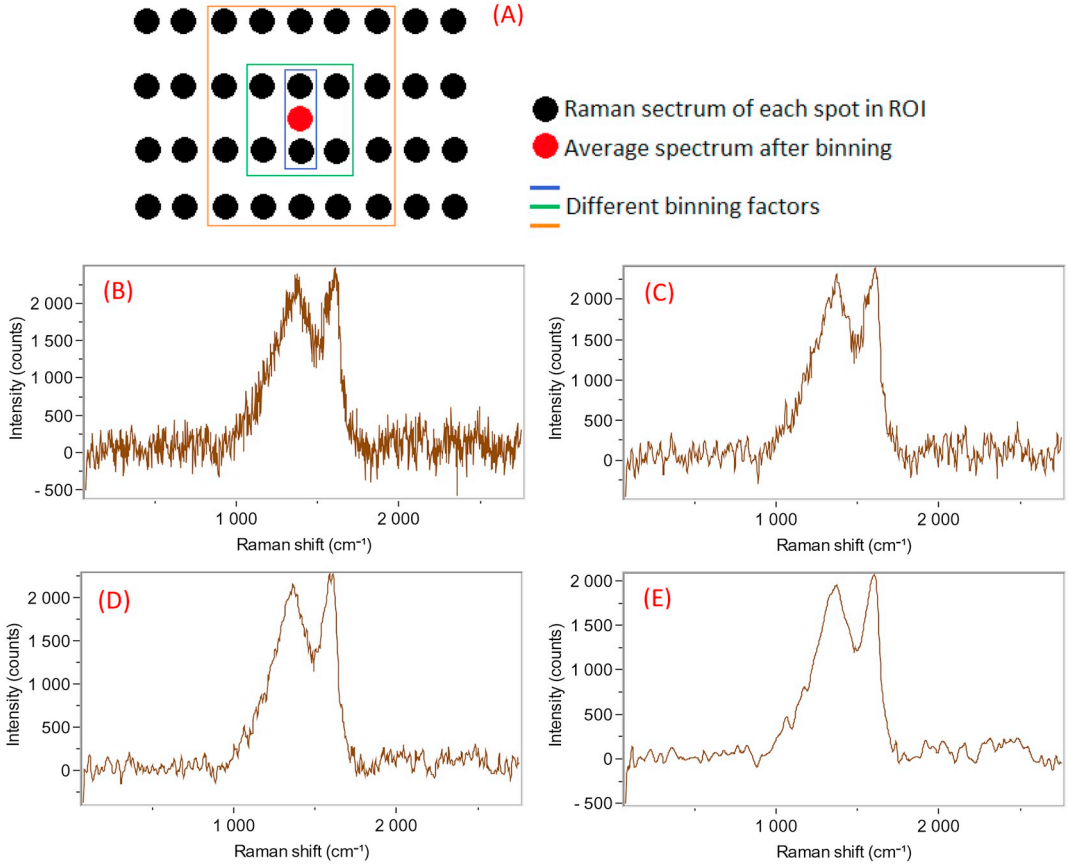

Fig. 4. (A) schematic of binning; (B) single spectrum; (C) binning factor of 4; (D) binning factor of 8; (E) binning factor of 20. Note the increase in signal to noise ratio and correspondingly losing spectral features by increasing binning factor.

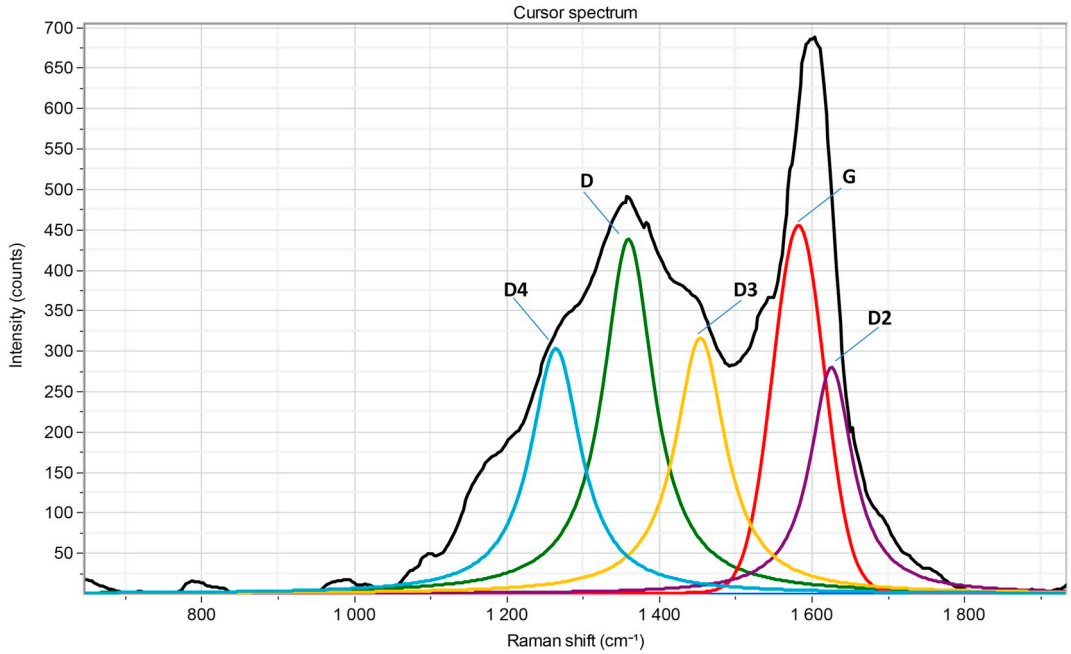

Fig. 5. Schematic of band peaking procedure using 5 peaks (D, G, D2, D3 and D4) and the experimental Raman spectrum (black). By adding more peaks, the reconstructed spectrum is more similar to experimental results and the $\chi 2$ value is reduced.

temperature conditions. Michels et al. (1995) discussed the effects of effluents and water pressure on oil generation during confined pyrolysis. Lewan and Ruble (2002) showed that there is no correlation between OM kinetic parameters derived from open-system pyrolysis and HP. Pan et al. (2009, 2010) illustrated the impact of water on the organic carbon ratio and mineral acidity during the conversion process of OM to hydrocarbons. They concluded that organic matter maturation rate slows down when a large amount of water is present. Further, Lewan and Roy (2011) explained significant differences in the types of products when water is involved at higher thermal maturity, noting that water promotes thermal cracking of bigger molecules over cross-linking. Other researchers have investigated the role of clay minerals in maturation, crude oil formation, migration and accumulation (Curtis et al., 2012; Chen and Xiao, 2014; Wu et al., 2012; Zhu et al., 2013; Hu et al., 2014; Kadoura et al., 2016). Such studies illustrated that the composition of petroleum is modified by interaction of clay minerals, and also the presence of water affects the role of minerals in acid-catalyzed cracking of kerogen. Despite advances in our understanding of these interactions, mimicking the natural condition of kerogen conversion to hydrocarbon remains poorly understood.

In a molecule, atoms are connected by chemical bonds, and thus have periodic motions. These motions relative to each other are superpositions of normal mode vibrations with the same phase and normal frequency (Schrader, 2008). The most effective methods to observe vibrational spectra as a signature representing a specific chemical compound are infrared and Raman spectrometry.

Kelemen and Fang (2001) showed the application of Raman spectroscopy for studying thermal maturity of OM, particularly in Silurian and older rocks where vitrinite is absent. Other researchers also have used Raman spectroscopy to reveal structural changes in organic matter during maturation (Ferrari and Robertson, 2000; Jehlička et al., 2003; Quirico et al., 2005; Guedes et al., 2012, Liu et al., 2013). Khatibi et al. (2018a, b, c, d) showed the potential application of Raman spectroscopy in correlating Raman signals to geochemical and mechanical properties of organic matter. They explained that changes in Young's modulus are representative of molecular alterations happening through thermal maturation. The application of Raman spectroscopy in qualitatively predicting geochemical properties of organic matter in terms of Rock-Eval parameters has also been studied (Khatibi et al., 2018a, b). Although Raman spectroscopy suffers from strong fluorescence background noise for immature shale samples, Khatibi et al. (2018d) showed that solvent extraction will reduce the fluorescence background if combined with specific signal processing techniques.

In this study, heterogeneity within the organic matter, solid bitumen, as a result of thermal advance (natural and artificial) has been studied in the Bakken Formation source rock samples. All samples were evaluated by OM reflectance, programmed pyrolysis and Raman spectroscopy. Then, maturation paths of two groups of naturally and artificially matured samples were compared. Raman spectroscopy results showed that HP did not follow the same natural geological conditions in maturation rate. This study also demonstrates the potential of Raman

Table 2
Major D and G bands shifts for both artificially and naturally matured samples in this study derived from the average spectrum across the ROI.

	Sample No.	D band	G band	G-D band
Artificially matured sample by HP	HP1	1362	1600	238
	HP2	1363	1598	235
	HP3	1362	1601.5	239.5
	HP4	1358	1603	245
	HP5	1359	1602	243
	HP7	1363	1607	244
	HP8	1357	1604	247
Naturally matured samples	Well 1	1367	1585	218
	Well 2	1367	1587	220
	Well 3	1360	1591	231
	Well 4	1354	1591	237
	Well 5	1359	1594	235
	Well 6	1357	1601	244

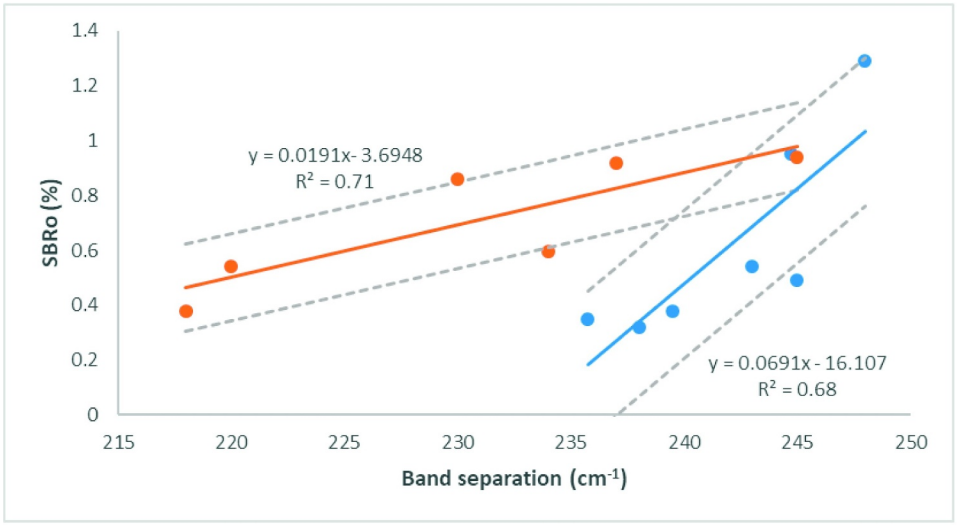

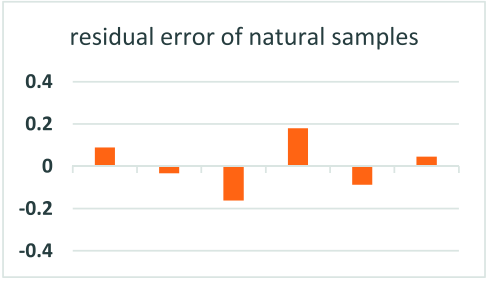

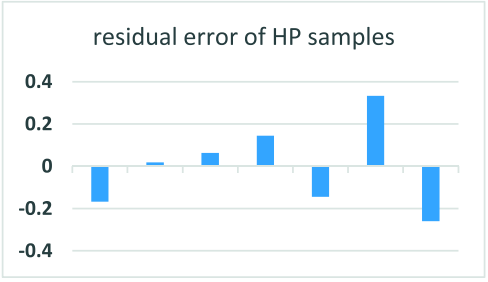

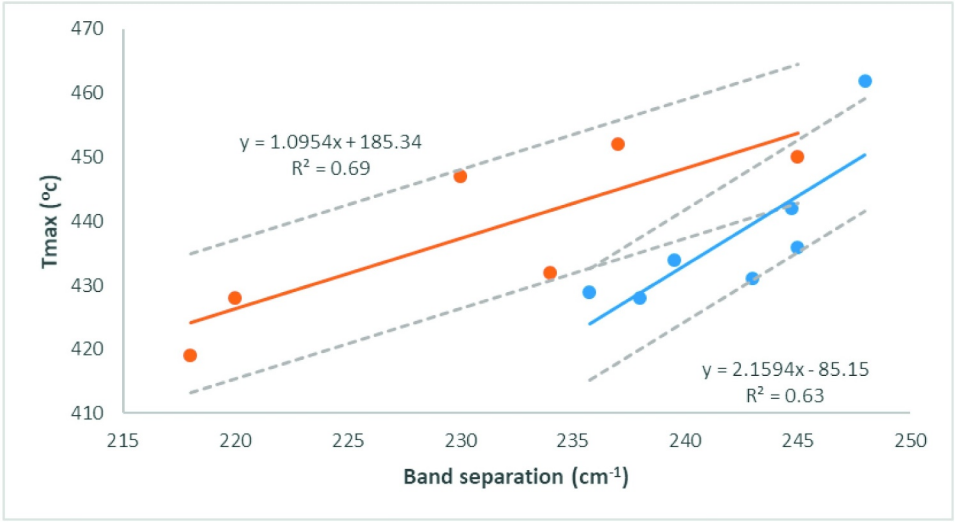

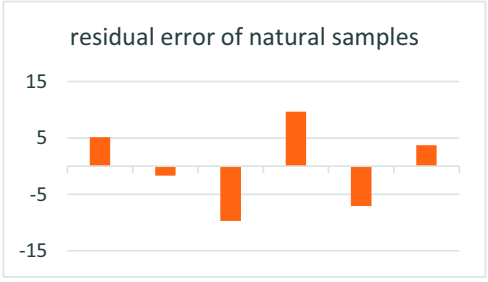

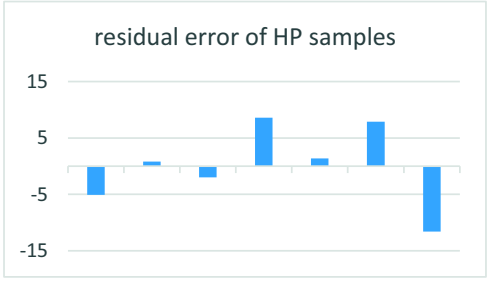

Fig. 6. SBRo and Tmax (as maturity indicators) vs. band separation along with 95% confidence interval of regression and residual error profile for each sample set. The 95% confidence interval defines a range of values that the population mean is covered with 95% of certainty. Note the consistent increase of band separation with increasing thermal maturity. Trendlines for HP and naturally matured samples along with their corresponding correlation coefficients are shown on each plot. Orange represents naturally matured samples and blue represents HP samples. (For interpretation of the references to colour in this figure legend, the reader is referred to the web version of this article.)

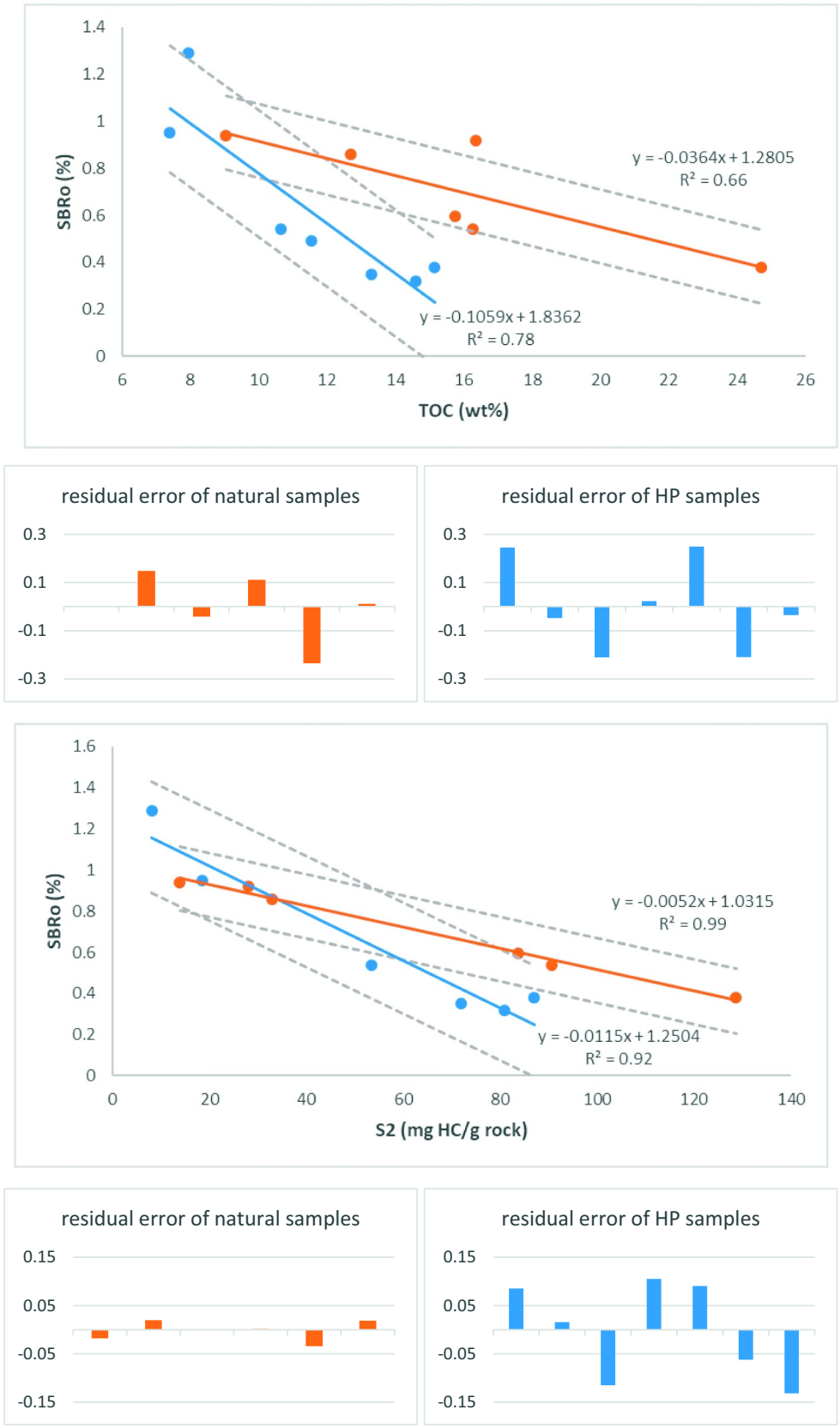

Fig. 7. (top) %SBRo vs. TOC; (middle) %SBRo vs. S2; (bottom) %SBRo vs. HI along with 95% confidence interval of regression and residual error profile. For each parameter plotted vs. %SBRo, trends are different for artificially and naturally matured samples. Orange represents naturally matured and blue represents HP samples.

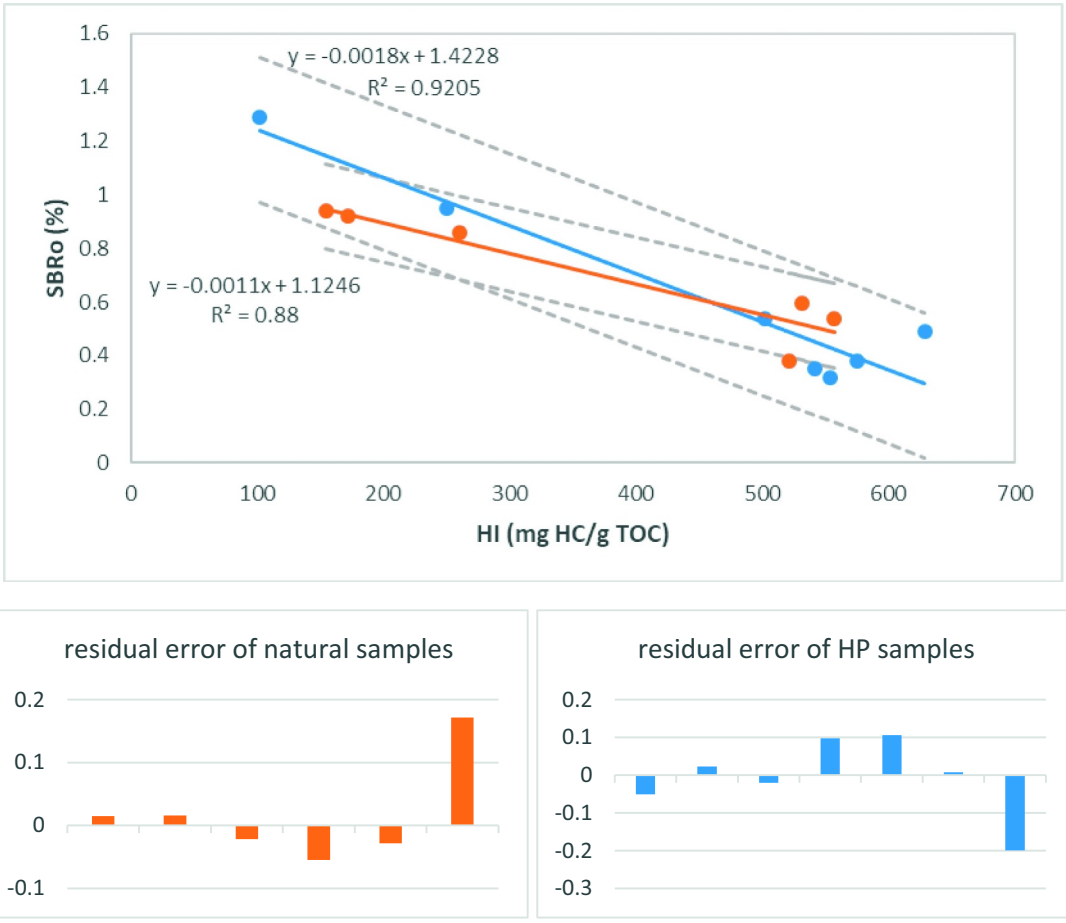

Fig. 7. (*continued*)

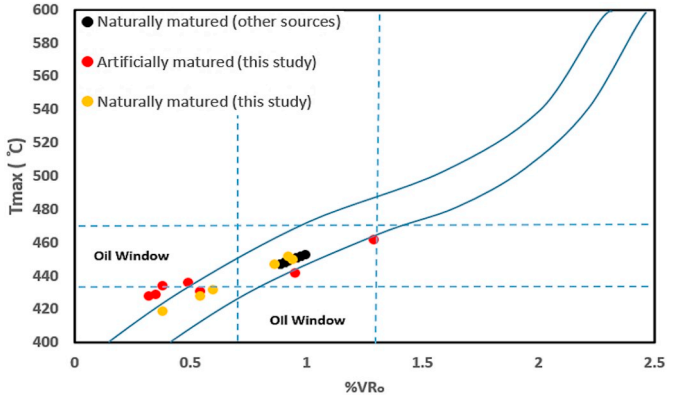

Fig. 8. Observed relationship between VRo% and T_{max} for natural samples (modified after Epistalié et al., 1985; Dembicki, 2016; Abarghani et al., 2018). It should be noted that measurements were based on %SBRo and were converted to vitrinite reflectance %VRo using the Jacob (1989) equation. Hydrous pyrolysis results (red circles) do not exactly follow the natural trend limits with dark blue curves. Light orange circles are naturally matured samples in this study, and black circles are naturally matured Bakken data extracted from Abarghani et al. (2018). (For interpretation of the references to colour in this figure legend, the reader is referred to the web version of this article.)

spectroscopy to analyze OM in terms of the spatial heterogeneity of solid bitumen. The results can enable us to build more accurate petroleum system models for shale plays, and also to develop protocols for pyrolysis to better resemble natural maturation conditions.

2. Samples and methods

Six samples were retrieved from the Bakken Formation as one of the most important source rocks in the Williston Basin, and consists of upper and lower organic-rich shales and a middle member of very fine-grained dolomitic sandstone and siltstone that was deposited during the Late Devonian and Early Mississippian Periods (LeFever et al., 2011). Williston Basin is an elliptical shaped depression in the western portion of North Dakota, the northeastern region of Montana and extends into parts of Saskatchewan and Manitoba in Canada, Fig. 1(A). Upper and lower shales that are the source for the Middle Bakken which is the reservoir, have the same lithofacies type (E.g. Angulo and Buatois, 2012; Zhang and Buatois, 2016) and are considered to have been deposited under relatively deep marine (> 200 m depth) anoxic conditions (Steptoe, 2012). Six samples at different stages of thermal maturity varying from 0.38 to 0.98%SBRo (Solid Bitumen reflectance) along with one immature sample (%SBRo of 0.32) that was artificially matured by HP to maximum maturity of 1.29% SBRo were used in this

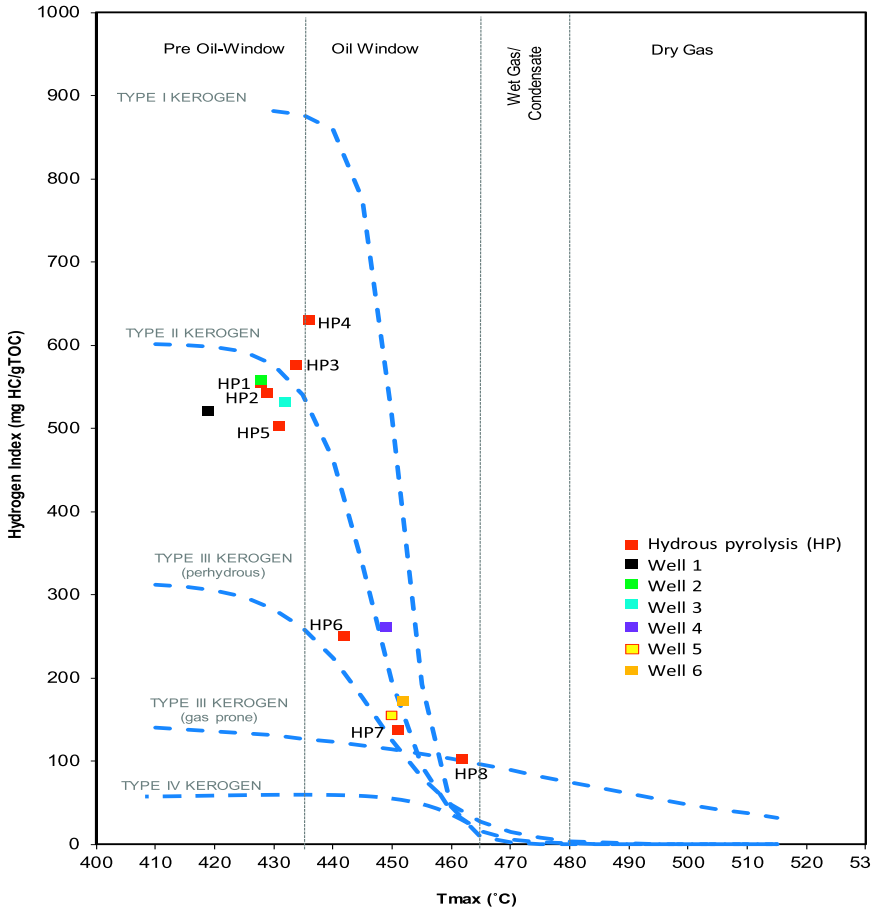

Fig. 9. Hydrogen index vs. T_{max} for kerogen typing. As seen all samples including naturally an artificially matured are approximately in type II kerogen (modified after Tyson, 1995).

study, Fig. 1(B). Geochemical analyses were performed by Rock-Eval 6, on both naturally and artificially matured samples, as summarized in Table 1.

Samples were prepared for petrographic analyses according to ASTM D2797 (ASTM, 2015a) wherein the rock particles were mounted in a thermoset plastic briquette, then ground and polished with successively finer abrasives until a 0.05-μm (μm) finishing stage. Solid bitumen reflectance analyses followed ASTM D7708 (ASTM, 2015b). In this technique, incident white light 546 ± 10 nm is reflected from solid bitumen positioned under the microscope crosshairs at 500× magnification, measured at a detector and compared to measured light reflected from a calibration standard. At least 20 measurements of solid bitumen reflectance were collected for each sample, with only 1 measurement per individual rock fragment. Since there was no reliable identification of primary vitrinite in the samples, mean random solid bitumen reflectance (%SBRo) is here reported in place of vitrinite reflectance, as practiced by many other workers (Jacob, 1989; Riediger, 1993; Jarvie et al., 2001; Hackley, 2012; Petersen et al., 2013; Valentine et al., 2014). Moreover, all analyses in the following sections were made on solid bitumen for better comparison purposes and consistency. Solid bitumen and vitrinite in shale are generally characterized as structureless gray substances in reflected white light, Fig. 1(C, D and E).

2.1. Hydrous pyrolysis

In order to perform hydrous pyrolysis on the immature sample and generate results comparable to the natural maturation sequence, the sample was first homogenized (broken to smaller pieces and thoroughly mixed). Homogenization was performed to make sure every portion is representative of the same original sample. Then, each part was taken through the HP process at elevated temperatures (300–360 °C) based on the method of Lewan (1993, 1997) in which crushed rock samples (2–4 g) were loaded into reactors and covered with de-ionized water. The amount of water should cover the sample and also be in contact with it constantly at the maximum temperature for each step of the experiment. The amount of rock and water added to each experiment were calculated from rock densities, reactor internal volumes, and steam tables as described by Lewan (1993). The stainless steel (SS-316) SwageLok™ mini-reactor vessels [25–35 ml (mL) internal volume] were assembled from 1.5-in. tubing caps and plugs, sealing with ~270 ft-pounds torque using Fel-Pro C5-A copper-based anti-seize thread lubricant. Once the reactor was sealed, it was placed into a gas chromatograph oven, and isothermally heated for 72 h. at 300–320–340-350-360 °C. It may take around 5–10 min for the oven to reach the experimental temperature which was not included in the main course of experiment durations. Pyrolyzed rock residues were removed and rinsed with acetone and then vacuum-dried overnight prior to preparations for further analyses.

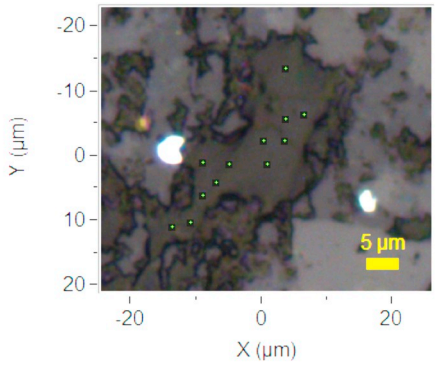

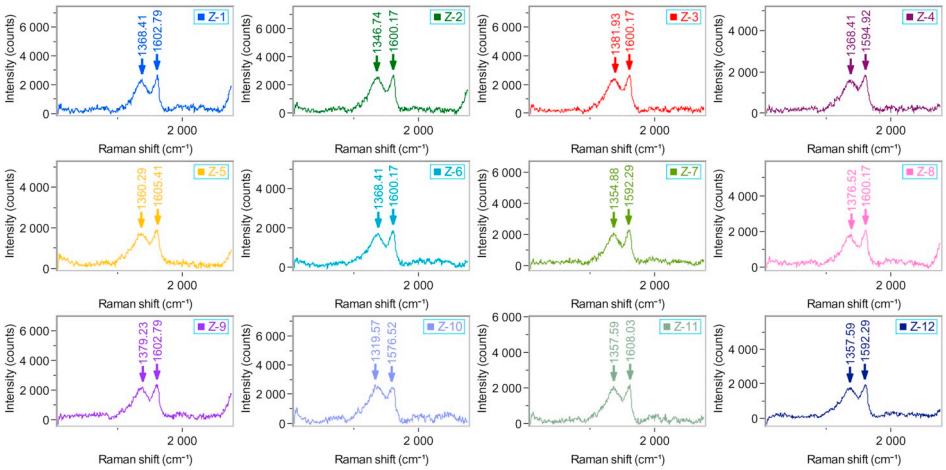

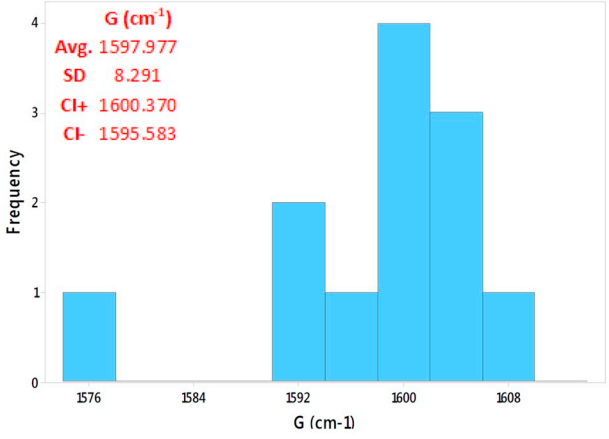

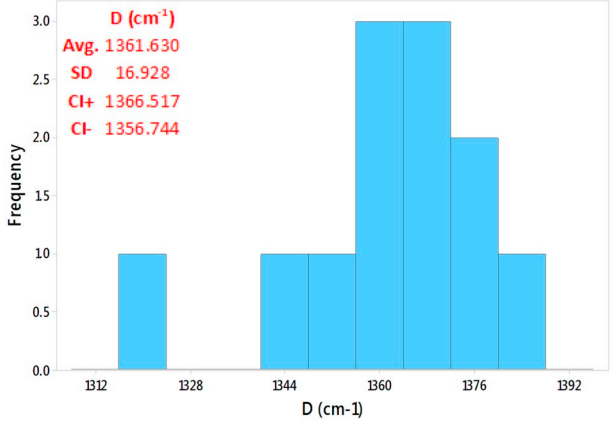

(caption on next page)

Fig. 10. sample HP1 with 0.32%SBRo: (top) Showing spots selected for averaging Raman signals (each green circle has about 3 3.6 μm^2 area); (middle) Raman spectra of corresponding spots; (bottom) Histogram of D and G bands position along with the statistical information of Avg.: average, SD: standard deviation, CI+: upper bound of confidence interval and CI-: lower bound of confidence interval. Bin sizes were defined based on Deviant (2011), range of data divided by number of bins.

2.2. Raman spectroscopy

To generate the Raman spectrum, we illuminated the sample surface with monochromatic laser light. Raman mapping mode was acquired on the region of interest (ROI) where organic matter (solid bitumen) was detected. As the probe scanned the area, 1000 points were collected (2 spectra per 1 μm^2), Fig. 2. The power of laser that was used for the acquisition of Raman data was 1 mW (1% of total laser power), with 1 s acquisition time, 3 s of accumulation which led to 3 mW.s of the energy dumped onto the surface of the sample. In terms of spectral precision, the grating (1200 grating/mm) was not moved from one spot to another; therefore, there was not any change in the spectral calibration. Moreover, the Raman spectrometer was calibrated before each data acquisition session using the 520 cm^{-1} Raman band of a silicon reference sample. The Si Raman band is an adjustment to an overall calibration of the spectrometer made with atomic emission lamps over the entire working spectral range of the spectrometer.

The benefit of using mapping mode is that statistical analysis can be used to estimate the shift of the major Raman bands of organic matter more accurately in microscale instead of acquiring a single Raman spectrum to represent the whole ROI. Furthermore, heterogeneity of OM composition can also be evaluated since a larger area is surveyed with a high spatial resolution. Moreover, one of the most important challenges regarding Raman spectroscopy is the fluorescence background which masks the Raman signal (Zhou et al., 2014; Myers et al., 2017). This issue is more critical while evaluating lower maturity samples due to the presence of high fluorescence intensity in OM, which is reduced at higher maturity (Lünsdorf, 2016; Sauerer et al., 2017). An appropriate processing technique can notably reduce the fluorescence background levels. For this purpose, a same polynomial baseline curve was fitted to the whole spectrum (from 50 cm^{-1} to 2750 cm^{-1}) (Fig. 3-left), which was the long wavelength function of the fluorescence, and then was subtracted from the spectrum (Fig. 3-right). Lower order polynomial functions are less flexible to adapt to the data and may not be able to include highly fluctuating backgrounds. Using this mathematical approach provides a flat zero baseline spectrum in order to pick Raman band positions in a more straightforward manner.

To improve signal to noise ratio (S/N) during Raman acquisition a binning procedure was used. In this process, a number of adjacent spectra (binning factor) in the ROI were co-added to increase the signal to noise ratio as displayed in Fig. 4. However, while using the binning factor, one should be cautious to avoid losing spectral features because of large binning. All spectra were collected with a frequency-doubled Nd:YAG 532 nm laser and the data were processed with the same background noise subtraction method explained earlier. Using 532 nm excitation with the MPlan 50× objective results in the beam diameter of 860 nm or 0.86 μm. The instrument was equipped with a 50× long working distance objective to easily locate the spot for Raman signal acquisition. Scan range of the instrument in mapping mode was 120 μm × 120 μm with a step size of 1.5 μm.

It should be mentioned the sample for thermal alteration were checked by viewing spectra in 1-second real-time display and setting the laser power such that no changes in the spectra occurred over at least 20 s of laser illumination prior to acquisition of a spectrum. The stable spectrum throughout illumination indicated that no burning was occurring over that time period. Furthermore, the samples were viewed by white reflected light microscopy after the measurement looking for any visible signs of sample burning. The absence of any change in the appearance of the sample after laser illumination indicated that no burning had occurred.

To characterize Raman spectral parameters such as peak position, intensity and area, a curve-fitting step should be performed. In this method, the experimental Raman spectrum was reconstructed by deconvolving overlapping peaks such that the summed spectrum of individual peaks matches the experimental data. A mixed Gaussian-Lorentzian peak morphology was used with 150 iterations until the best fit was achieved. The quality of fit was evaluated visually from the residual spectrum and numerically by the standard error ($\chi 2$), where smaller $\chi 2$ corresponds to a better reconstruction as outlined by previous researchers (Quirico et al., 2005; Sadezky et al., 2005; Bonoldi et al., 2016; Lupoi et al., 2017). Researchers often fit 5 peaks for OM evaluation in shale plays (Schito et al., 2017; Sauerer et al., 2017; Schmidt et al., 2017; Cheshire et al., 2017; Lupoi et al., 2017), known as D, G, D2, D3 and D4 as shown in Fig. 5. In this study, 5 fits were fitted as well, but major bands (D and G) were only considered in the results (Table 2) as the molecular significance and appearance of the minor bands (D2, D3 and D4) are not well understood (Beyssac et al., 2003). Please note that the bands in Table 2 were derived from the average spectrum across the ROI.

3. Results and discussion

LECO total organic carbon (TOC) values for the samples vary from 7.39 wt% to 24.71 wt%. The higher S1 values in the lower maturity samples could be the result of a) in-situ hydrocarbon generation, b) contamination by oil-based mud (in the naturally-matured samples), or c) a combination of both (in the naturally matured samples). Some of the samples exhibit higher S2 values (33.01–128.71 mg HC/g rock), indicating excellent remaining hydrocarbon generating potential. The high Hydrogen Index (HI) values for the immature samples represents oil-prone organic matter. TOC and S2 (as well as HI) show a decrease with increasing thermal maturity. The Production Index (PI) values are also low, which is common for samples that are immature to marginally mature.

Previous studies have reported that thermal maturity causes a logical variation in the positions, separations and other important parameters of Raman spectral bands for organic matter (Spötl et al., 1998; Ferrari and Robertson, 2000; Kelemen and Fang, 2001; Sauerer et al., 2017; Khatibi et al., 2018a, b). Moreover, similar studies have been conducted on solid bitumen in particular and the results found to be in agreement with the trend that was observed on the organic matter (Jehlička et al., 2003; Court et al., 2007; Zhou et al., 2014).

It is well known that with increasing kerogen maturity, aromaticity increases with concurrent loss of H, O, N and S content (Tissot and Welte, 1984; Tyson, 1995). Such compositional evolution can be reflected in both bulk geochemical analysis (programmed pyrolysis) and molecular scale as measured by Raman spectral character (Kelemen and Fang, 2001; Quirico et al., 2005; Sauerer et al., 2017). In Raman spectra, the major bands of D and G represent the aromaticity level of organic matter and the level of disorder in molecular structure of organic atoms. Therefore, Raman spectroscopy can detect different levels of thermal advance based on the response from these molecular signals.

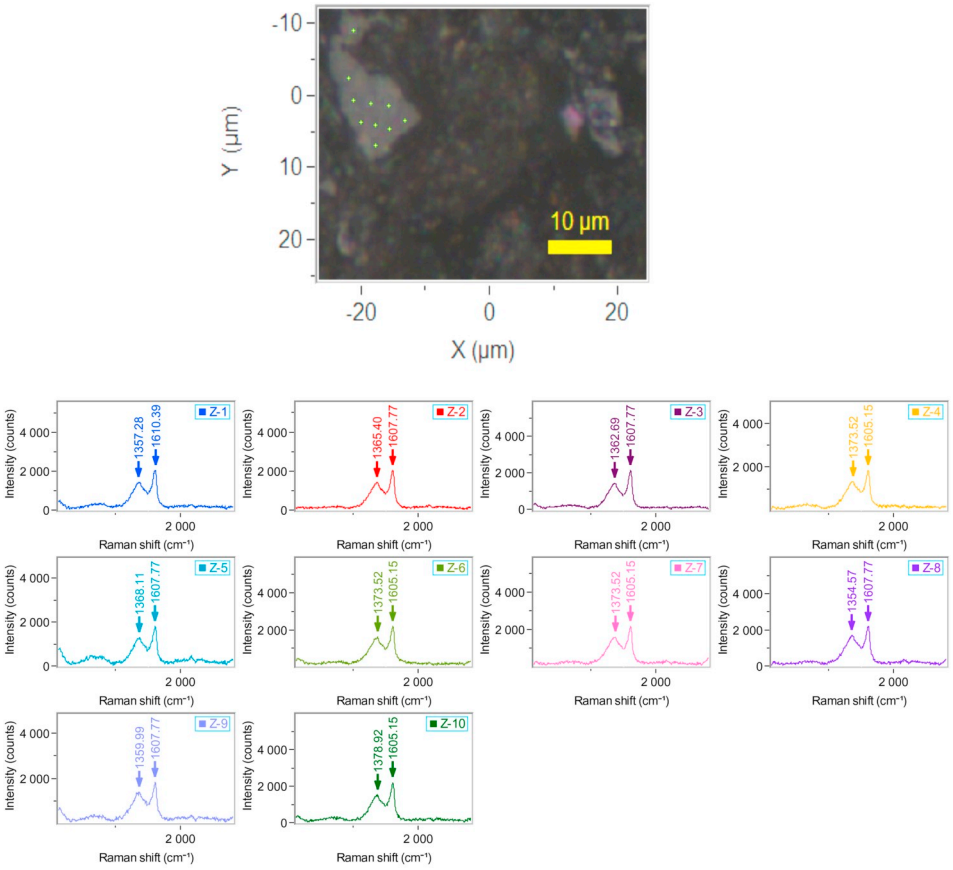

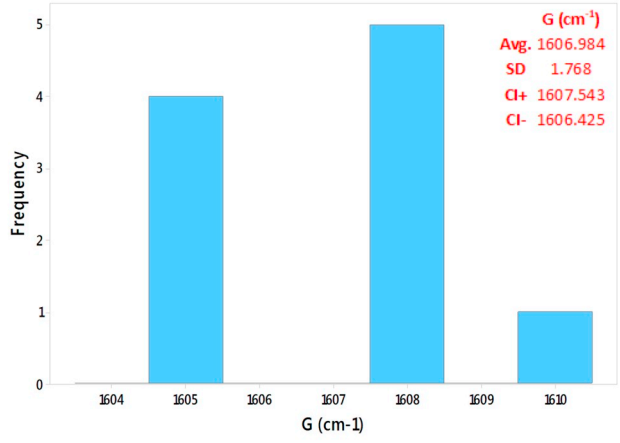

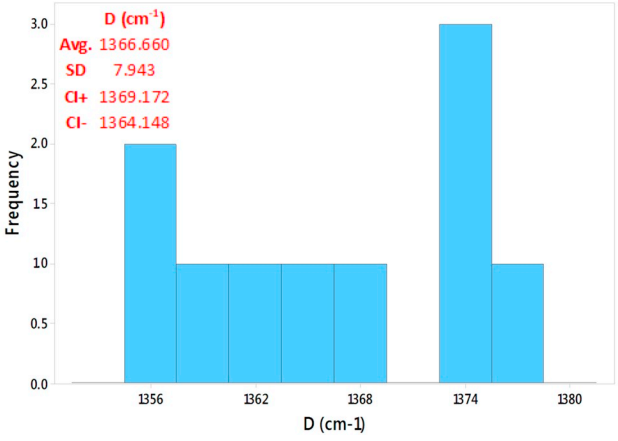

(caption on next page)

Fig. 11. Sample HP6 with 0.95%SBRo: (top) Showing spots selected for averaging Raman signals; (middle) Raman spectra of corresponding spots; (bottom) Histogram of D and G bands position along with the statistical information of Avg.: average, SD: standard deviation, CI+: upper bound of confidence interval and CI-: lower bound of confidence interval. Bin sizes were defined based on what is discussed by Deviant (2011), range of data divided by number of bins.

A well-known increase in the G-D band separation with maturity (up to dry gas window) is due to the shift in the D band position towards lower wavenumbers and the G band towards higher wavenumbers (Kelemen and Fang, 2001). These shifts are attributed to the increase of larger aromatic clusters and better ordered-structure kerogen in terms of the existing organic compounds (Schito et al., 2017). Fig. 6 shows a cross-plot of SBRo vs. band separation and Tmax vs. band separation along with 95% confidence interval (CI) of the regression line and corresponding error profile (residuals) for both naturally (orange) and HP samples (blue). Confidence interval represents the range that the mean response is likely to fall, given the specified settings of the predictors (Hicks and Irizarry, 2018). Residual error is the difference between the observed value and the estimated value by the regression. If the points in a residual plot are randomly dispersed around the horizontal axis, a linear regression model is appropriate for the data (Lawson and Erjavec, 2000) which is the case in the results from this study and observed errors. A similar plot was also shown by Zhou et al., (2014) which showed natural and artificially matured samples do not show the same trend when plotting full width at half maximum (FWHM) of D band vs. SBRo.

Functions fitted to the two separate datasets (naturally and artificially matured samples) show visibly distinct slopes. It is known that different organic matters mature at various rates due to the presence of specific functional groups (Yang et al., 2017) with different kinetic parameters. To remove this effect, as mentioned earlier, solid bitumen was used exclusively in our study. Lewan and Ruble (2002) concluded kinetic parameters derived from HP would determine geologically significant differences between source rocks bearing different kerogen types, conversely to open-system pyrolysis. This difference in maturation trend is also observed for changes in bulk measurements such as TOC, S2 and HI, as shown in Fig. 7. Relationships between measured % VRo and programmed pyrolysis values have been introduced in previous studies (Olson, 2008; Klentzman, 2009; Hackley et al., 2015). For example, Espitalie et al. (1985), Dembicki (2016) and Abarghani et al. (2018) investigated different geochemistry datasets from the Bakken and presented a 'normal' kerogen maturation pathway for T_{max} as a function of %VRo as shown in Fig. 8. Fig. 8 also depicts artificially matured samples of this study do not follow the trend of natural ones in T_{max}-VRo space which is also reflected in the Raman spectra (Fig. 6). This difference is mainly inferred to the fact that HP residues are still reactive. Therefore, although the SBRo of HP samples are the same as the natural sequence, their compositions are not. Mumm and Inan (2016) presented different trends of maturity vs. band separation for different OM including Type II, III, coal and bitumen samples. They also observed, for the same reflectance range, the results for different types of organic matter could vary. They assumed such discrepancy might originate from the experimental setup, while part can be attributed to dissimilarities in structural composition of these samples which has been reflected in Raman signals. Ferralis et al., (2016) also used Raman spectroscopy in a novel quantitative method to correlate Raman signals to the microchemistry of carbonaceous materials through the elemental H:C ratio. Thus, they detected different trends for HP and naturally matured samples reflecting differences in structural characteristics of each set of samples.

This discrepancy in the rate and path of maturation for naturally and artificially matured samples can be referred to a separate reaction medium between HP and natural geologic processes of maturation. The importance of reaction medium (defined as the effect of water, minerals, heating rates, and pressure on organic maturation in HP) has been discussed extensively (Monthioux and Landais, 1987, Monthioux, 1988; Michels and Landais, 1994; Mansuy et al., 1995; Dieckmann et al. 2000; Bajc et al., 2001; Pan et al., 2009, 2010; Liang et al., 2015). Water as the exogenous source of hydrogen seems to have an important role in oil generation and simulation of the natural reaction medium (Lewan, 1997), whereas the dominant reaction pathway in the absence of water is formation of pyrobitumen due to C—C bond cross linking. Additionally, in the presence of water, the primary reaction pathway is formation of saturate-enriched oil due to thermal cracking of C—C bonds (Monthioux et al., 1985). Mineral acidity also increases maturation rate as well as affecting the byproducts from maturation (Pan et al., 2009), while impermeability of fine-grained sediments prevents forward reaction progress (McTavish, 1998; Li et al., 2004; Hao et al., 2007). Several researchers have investigated the effects of reaction medium in formation rates of hydrocarbon (Cramer et al., 1998, 2001; Tian et al., 2007). Definitely based on the extent of kerogen conversion, the amount of trapped bitumen in the pyrolyzed and naturally matured samples might be also different. Monthioux et al. (1985) showed natural maturation is best simulated when pyrolysis is performed under confined conditions in which free volume or diluting inert gas is not present. Kinetic constants of geochemical reactions derived from HP has shown that reaction mechanisms in nature and in the laboratory are distinctly different (Mackenzie and McKenzie, 1983; Rullkotterand and Marzi, 1988).

Therefore, it can be concluded that the presence of water, minerals, heating rates, and pressure are all affecting the maturation paths of organic matter in addition to the variability of the macerals present. Kinetics of hydrocarbon generation and maturation all are dependent upon molecular structure of kerogen (Tegelaar and Noble, 1994; Behar et al., 1997; Killops and Killops, 2013). This dependency can also be extended to nanomechanical and nanoporosity evolution of organic matter (Chen and Xiao, 2014; Liu et al., 2017, 2018). In this regard, bulk chemical measurements suffer notably from representing molecular structure of kerogen, a property which is not known fully. For instance, although Rock-Eval data and (Pseudo) Van Krevelen diagram (Van Krevelen, 1993) as seen in Fig. 9, exhibits very similar organic matter type/origin, detailed molecular analyses of the samples are proving otherwise.

To date, HP/AHP are known to be the most suitable simulation methods for thermal maturity progression. However, as it was discussed there exist several parameters that should be known prior to experiments to make them mimic natural maturity pathway. For example, a better understanding of molecular structure of OM that can be detected by Raman spectroscopy in a fast and accurate way using methods provided by Ferralis et al. (2016) and Khatibi et al. (2018d) can provide a better insight into the samples variability to set HP/AHP parameters. In order to achieve this goal, it is suggested first, different HP/AHP experiments to be performed on immature samples from the same source rock, then compare the cross-plot of Raman bands vs. maturity for both naturally and artificially matured samples as shown in Fig. 6. If the fitted curves on both datasets exhibit the same slope, it can be concluded that HP/AHP has followed natural geologic processes for thermal maturation, which was not the case in this study. In conjunction with Raman spectroscopy, variations in the extent and timing of petroleum generation in pyrolysis can also be compared using gas

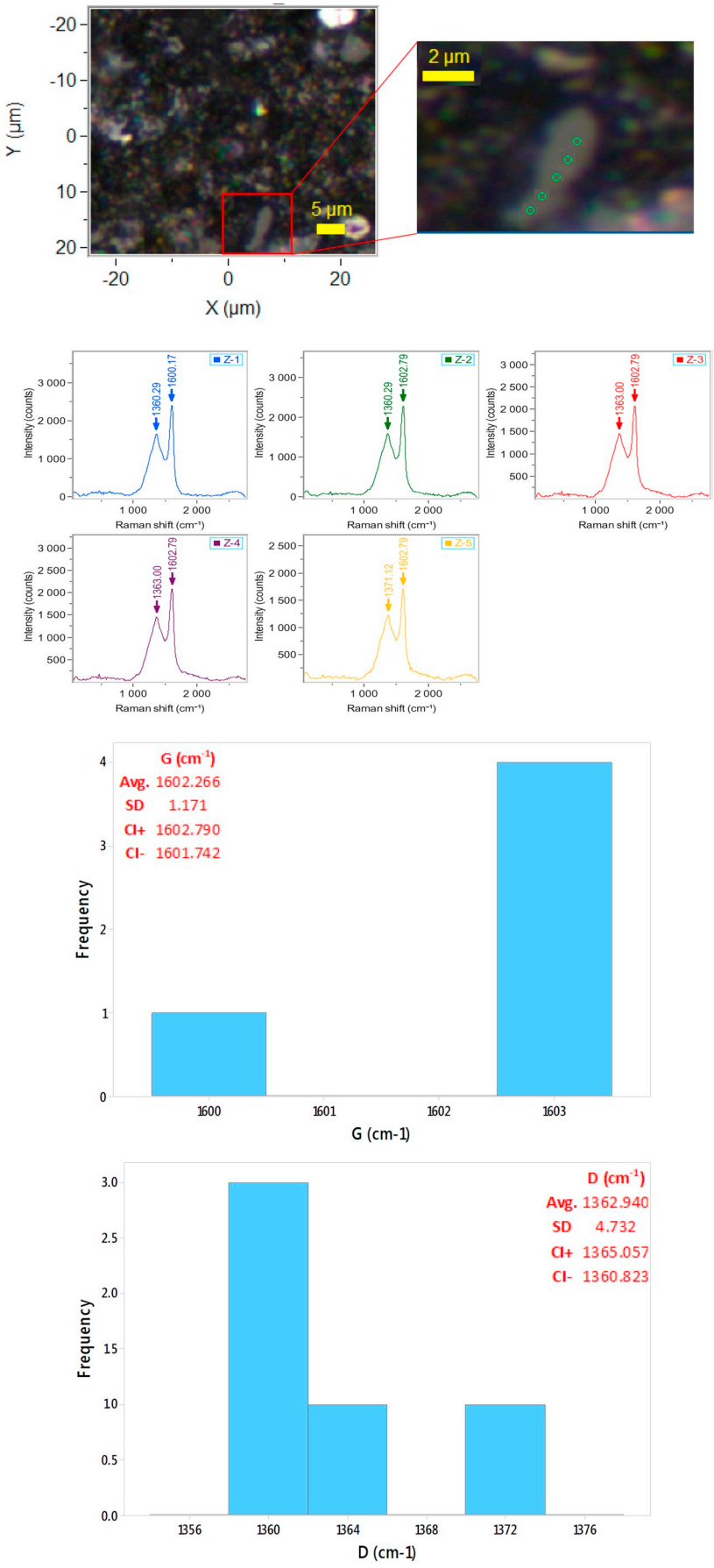

(caption on next page)

Fig. 12. Sample HP8 with 1.29%SBRo: (top) Showing spots selected for averaging Raman signals; (middle) Raman spectra of corresponding spots; (bottom) Histogram of D and G bands position along with the statistical information of Avg.: average, SD: standard deviation, CI+: upper bound of confidence interval and CI-: lower bound of confidence interval. Bin sizes were defined based on what is discussed by Deviant (2011), range of data divided by number of bins.

chromatography–mass spectrometry (GC–MS) at the bulk scale to find the optimum method in which natural maturation is better followed.

3.1. Heterogeneity

Spatial variability in chemical structures and other properties of organic matter can be distinguished using Raman spectral mapping mode. In this method, regions on the surface of solid bitumen were selected and their corresponding spectra were analyzed, as presented in Figs. 10 to 12. To avoid the inconsistency of different biogenic sources and natural variability, the following results are based on HP samples and Raman spectra were obtained only from solid bitumen particles. In order to minimize the effects of technical detail (excitation laser energy, processing steps, sample preparation etc.) the same procedures were used for all samples.

It has been shown that carbonaceous matters are sensitive to the polishing process, and the effect is significant (Lünsdorf, 2016). The excitation wavelength might also affect the Raman results, so in order to avoid such bias, the same wavelength for each and all sample surfaces was used to acquire Raman spectra. Moreover, short laser excitation wavelengths (488 nm and less) are usually used for Raman acquisition of organic matter to invoke far less fluorescence background noise (Lünsdorf, 2016), which is also the case in this study. Raman spectral mapping mode showed that different locations within the same solid bitumen particle did not necessarily present the same Raman spectral characteristics. This variation in the spectra is represented herein by G-D band separation as well as the corresponding statistical details in the tables representing the histograms (Figs. 10 to 12). Please note bin size and the number of the bins in Figs. 10 to 12 were decided based on the discussion by Deviant (2011). If it is assumed that polishing and laser wavelength had negligible effects on collected data, it can be concluded that the variability in Raman spectral results might be due to the heterogeneity of organic matter in terms of chemical composition. Results are also in agreement with recent research that was performed by Jubb et al., (2018) who detected high variability in the Raman response across a < 5 μm spatial distances of single OM in shale samples.

Moreover, as thermal maturity advances, observed variation in G and D band parameters reduce for different locations within the same solid bitumen particle. This observation suggests that heterogeneity of organic matter decreases with increasing thermal maturity; note the decrease in standard deviation values or confidence interval range (upper and lower bounds of confidence interval define a range of values that we can be 95% certain contains the population mean) for different samples in Figs. 10 to 12. Similar results are also reported by Jubb et al., (2018) for Niobrara shale sample that OM chemical heterogeneity is lost for samples with higher thermal maturity. This can be explained by increase in aromaticity, and heteroatoms expulsion; therefore, no matter its origin or type, OM tends to become graphite-like at higher maturity (Tuinstra and Koenig, 1970; Waples, 1981; Tissot and Welte, 1984; Tyson, 1995; Ferrari and Robertson, 2000; Quirico et al., 2005; Potgieter-Vermaak et al., 2011; Zhou et al., 2014; Lünsdorf, 2016; Mumm and Inan, 2016; Schito et al., 2017). This is also in accordance with the original Van Krevelen diagram in which all kerogen types converge to the origin as their composition and structure become similar when thermal maturity is increased (Killops and Killops, 2013).

Raman band separation maps for solid bitumen particles in Figs. 10–12 are displayed in Fig. 13. Table 3 also shows the corresponding standard deviation (SD) and coefficient of variation (CV) of spectra for each sample. Results are showing decreasing of band separation variability with increasing maturity. Interpolation method for surface data generation is performed using the minimum curvature method which uses an operator that keeps the surface data smooth with a minimum amount of bending, while attempting to honor the data as closely as possible (Yang et al., 2004; Amorin, 2009). It can be seen, across the surveyed solid bitumen particles, band separation (G-D) exhibits variations which might represent changes in chemical composition, matrix effects (specifically near the edge of the grain) and/or surface quality. In order to demonstrate these variations in Raman signals across each surveyed particle more clearly, CLS (classical least square) fitting was used as a multivariate decomposition technique. This procure was used to calculate the contribution of the reference spectra in the same size area to create a profile based on the similarity of each spectrum to the reference spectrum. The reference spectrum was selected in the middle of each sample to be far from edges, Fig. 14. From the figures it can be concluded: by increasing maturity the magnitude of fluctuations in band separation is decreasing, and distribution of band separation will become more uniform throughout the solid bitumen particle which might denote advancement towards compositional homogeneity. Similar results were observed by Lünsdorf (2016) and Jubb et al., (2018).

This representation of heterogeneity within a solid bitumen phase may explain other heterogeneous behaviors such as mechanical properties of OM. It has been shown in the literature, as thermal maturity increases, mechanical properties (e.g., elastic modulus) of organic matter alter (Eliyahu et al., 2015; Li et al., 2018a, b). It can be described as in immature source rocks the OM appears to surround other minerals, becoming a load-bearing part of the rock framework (Liu et al., 2017, 2018; Zargari, 2015). Conversely, by increasing the maturity, kerogen becomes more isolated between the other grains and results in an increase in its Young's modulus (Zargari, 2015; Dietrich, 2015). In terms of molecular structural evolution, organic matter transforms gradually from chaotic and mixed-layered to a better-ordered aromatic molecular structure (Beyssac et al., 2003; Quirico et al., 2005; Khatibi et al., 2018d). This reasoning is also consistent with the previous paragraph regarding decreasing of heterogeneity of molecular structure by increasing maturity.

The continuous chemistry information obtained from solid bitumen particles by Raman spectroscopy may have the potential to enhance conventional petrographic or bulk geochemistry analytical approaches. For example, Raman spectroscopy has the benefit of minimal sample preparation (It can be done on sample chips as well) in a non-destructive manner and fast acquisition by pinpointing the organic matter and illuminating by proper laser wavelength. Additionally, the cross-plot of SBRo with Raman data, can enable us to adjust the condition of pyrolysis to make it resemble natural maturation pathways more accurately at the small scale and confirm it with bulk measurements in programmed pyrolysis. To do so, several HP and AHP setups can be performed and the cross-plot of Raman bands vs. maturity should be compared to naturally matured samples. Moreover, detecting heterogeneity and providing maturity maps can also be a tool for further understanding of kerogen characteristics. The latest requires extensive sample collection (sample number/ft) and spectroscopy study both laterally and vertically from source to reservoir. To accomplish more

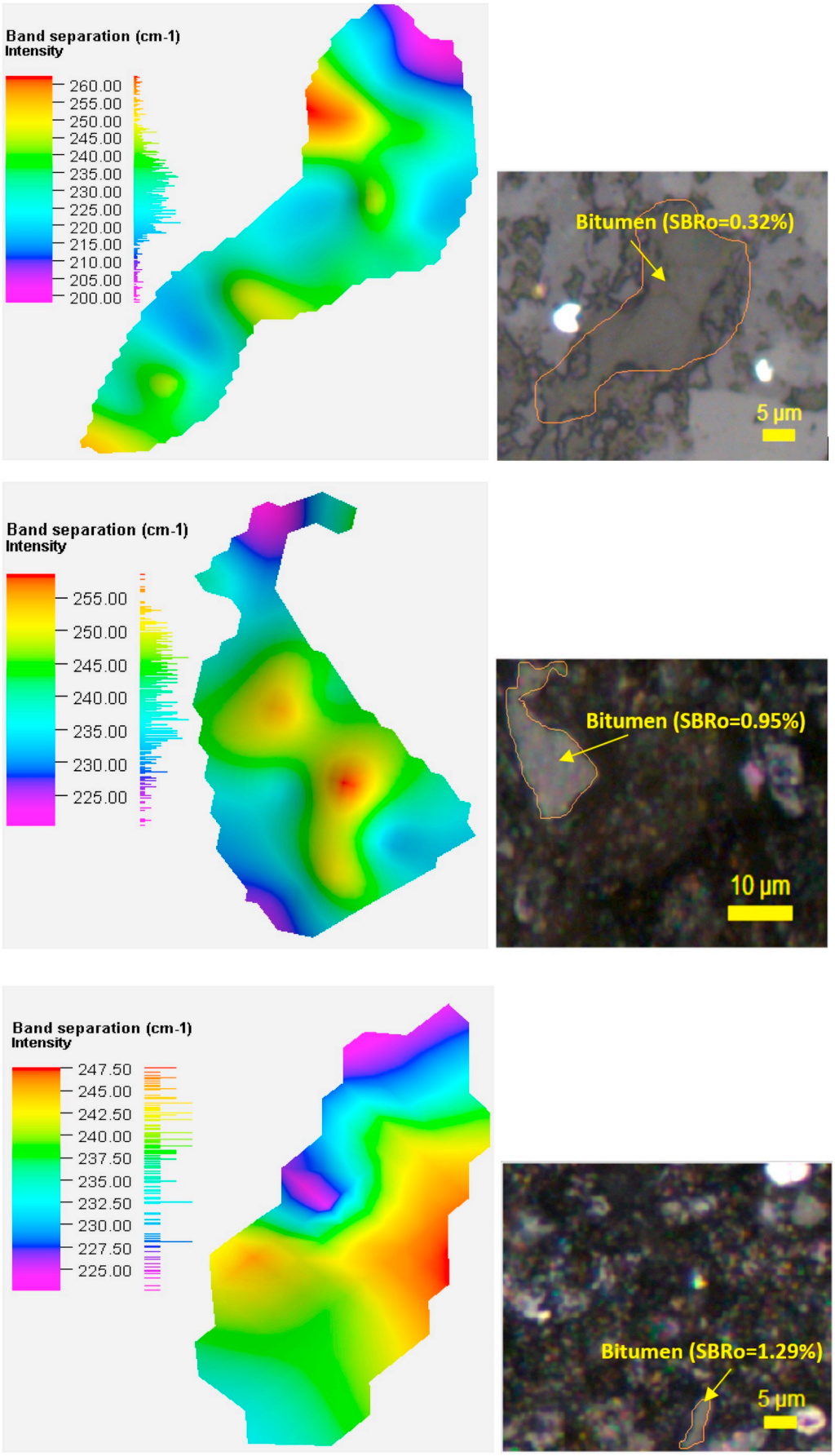

(caption on next page)

Fig. 13. Raman map of a bitumen corresponding to Figs. 10 to 12 (HP 1, HP6 and HP8, respectively). Note the changes of band separation indicating changes of chemical composition of the solid bitumen. As seen, variation of band separation is reducing by increasing maturity. Please note bar graphs next to colour scales shows the frequency of each band separation.

Table 3
Standard deviation (SD) and Coefficient of variation (CV) of band separations for HP 1, HP6 and HP8 for the entire area of interest. As see, by increasing maturity, the measures of variability are decreasing. CV is useful for calculating the relative magnitude of the standard deviation when few data are available for different datasets.

Maturity of the sample	SD	CV
0.32	11.725	0.050
0.95	8.621	0.036
1.29	6.036	0.026

extensive results, this study will be continued by analyzing samples with a wider range of maturities, including different type of macerals, and complement our Raman data with Nano-IR measurements to give a better insight to heterogeneity of organic matters.

4. Conclusion

In this study, samples from the source rock of the Bakken Formation varying in depth and maturity were retrieved. One of the samples was then artificially matured through various stages of hydrous pyrolysis. Solid bitumen reflectance, programmed pyrolysis and Raman spectroscopy were performed on all samples to obtain general maturity, bulk geochemistry and chemical fingerprinting. In the next step, Raman signals were acquired on solid bitumen particles on HP samples (at each stage) to show the heterogeneity of organic matter more possibly due to chemical composition. In addition, Raman data revealed different maturation rates between natural and artificially matured samples. We understand that various parameters are affecting the path that leads OM towards higher maturity levels, however, the overall impact of all of them would be on the chemical structure of the remaining OM. This structural evolution can be detected by Raman spectroscopy as a whole at different maturity levels no matter the dominant underlying reason. Previous studies evaluated these governing factors separately whereas here, we were able to see a combined effect of them via Raman spectra. Based on the results the following conclusions are made:

- Raman spectroscopy was able to detect molecular alterations in the organic matter as it undergoes thermal maturity.
- Raman mapping mode provided a way to compare different OM solid bitumen particles in microscale in a continuous format at varying maturity levels.
- We found, HP although known as the best thermal maturity simulation method, did not necessarily follow natural maturation conditions. This was revealed by the cross-plot of Raman spectroscopy data vs. conventional geochemistry results. The result can help to propose protocols and adjust experimental parameters for HP based on those cross-plots for more accurate thermal maturity progression steps in the lab.
- Raman spectroscopy can reflect heterogeneity of organic matter at microscale which can also represent expected heterogeneity in geochemical and geomechanical properties of the OM.
- It was found as maturity increases, heterogeneity of organic matter decreases and Raman map of solid bitumen particle shows more uniform distribution of G-D band characteristics.

Acknowledgment

The authors wish to thank Dr. Thomas Gentzis and Dr. Humberto Carvajal-Ortiz from Core Laboratories in Houston, TX, for providing us with geochemistry data and fruitful discussions. We would like to also thank, North Dakota Geological Survey, Core Library, for giving us access to the Bakken core samples, particularly Jeffrey Bader, state geologist and director as well as Kent Hollands, lab technician. Finally, we would also like to thank Dr. Aaron Jubb at the USGS Eastern Energy Resources Science Center in Reston, Virginia for providing his constructive comments and reviewing this manuscript.

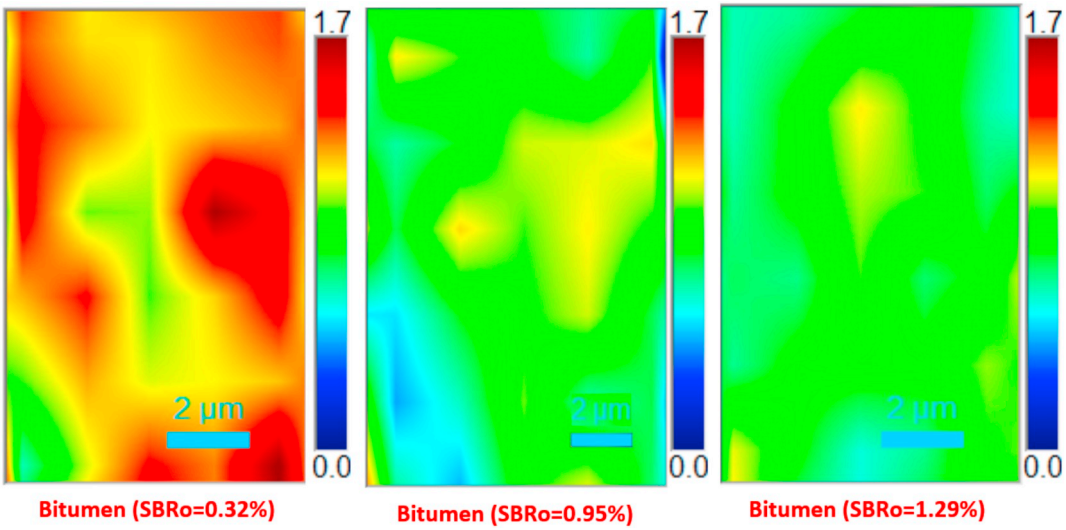

Fig. 14. Results of classical least square fitting procedure for three samples of HP 1, HP6 and HP8. A reference spectrum in the middle of the window is selected and similarity of each spectrum to the reference spectrum is shown. Higher values in the legend show higher dissimilarity.

References

Abarghani, A., Ostadhassan, M., Gentzis, T., Carvajal-Ortiz, H., Bubach, B., 2018. Organofacies study of the Bakken source rock in North Dakota, USA, based on organic petrology and geochemistry. Int. J. Coal Geol. 188, 79–93.

Amorin, Richard, 2009. "Application of Minimum Curvature Method to Well-Path Calculations". PhD Diss.

Angulo, Solange, Buatois, Luis A., 2012. Integrating depositional models, ichnology, and sequence stratigraphy in reservoir characterization: the middle member of the Devonian–Carboniferous Bakken Formation of subsurface southeastern Saskatchewan revisitedBakken Formation Reservoirs, Saskatchewan, Canada. AAPG Bull. 96 (6), 1017–1043.

Bajc, S., Ambles, A., Largeau, C., Derenne, S., Vitorović, D., 2001. Precursor biostructures in kerogen matrix revealed by oxidative degradation: oxidation of kerogen from Estonian kukersite. Org. Geochem. 32, 773–784.

Behar, F., Vandenbroucke, M., Tang, Y., Marquis, F., Espitalié, J., 1997. Thermal cracking of kerogen in open and closed systems: determination of kinetic parameters and stoichiometric coefficients for oil and gas generation. Org. Geochem. 26, 321–339.

Beyssac, Olivier, Goffé, Bruno, Petitet, Jean-Pierre, Froigneux, Emmanuel, Moreau, Myriam, Rouzaud, Jean-Noël, 2003. On the characterization of disordered and heterogeneous carbonaceous materials by Raman spectroscopy. Spectrochim. Acta A Mol. Biomol. Spectrosc. 59 (10), 2267–2276.

Bonoldi, Lucia, Di Paolo, Lea, Flego, Cristina, 2016. Vibrational spectroscopy assessment of kerogen maturity in organic-rich source rocks. Vib. Spectrosc. 87, 14–19.

Carvajal-Ortiz, H., Gentzis, T., 2015. Critical considerations when assessing hydrocarbon plays using Rock-Eval pyrolysis and organic petrology data: data quality revisited. Int. J. Coal Geol. 152, 113–122.

Chen, J., Xiao, X., 2014. Evolution of nanoporosity in organic-rich shales during thermal maturation. Fuel 129, 173–181.

Cheshire, Stephen, Craddock, Paul R., Xu, Guangping, Sauerer, Bastian, Pomerantz, Andrew E., McCormick, David, Abdallah, Wael, 2017. Assessing thermal maturity beyond the reaches of vitrinite reflectance and Rock-Eval pyrolysis: a case study from the Silurian Qusaiba formation. Int. J. Coal Geol. 180, 29–45.

Court, Richard W., Sephton, Mark A., Parnell, John, Gilmour, Iain, 2007. Raman spectroscopy of irradiated organic matter. Geochim. Cosmochim. Acta 71 (10), 2547–2568.

Cramer, B., Krooss, B.M., Littke, R., 1998. Modelling isotope fractionation during primary cracking of natural gas: a reaction kinetic approach. Chem. Geol. 149, 235–250.

Cramer, Bernhard, Faber, Eckhard, Gerling, Peter, Krooss, Bernhard M., 2001. Reaction kinetics of stable carbon isotopes in natural gas insights from dry, open system pyrolysis experiments. Energy & Fuels 15 (3), 517–532.

Curtis, M.E., Cardott, B.J., Sondergeld, C.H., Rai, C.S., 2012. Development of organic porosity in the Woodford Shale with increasing thermal maturity. Int. J. Coal Geol. 103, 26–31.

Dembicki, H., 2016. Practical Petroleum Geochemistry for Exploration and Production. Elsevier.

Deviant, S., 2011. The Practically Cheating Statistics Handbook–. Lulu. com.

Dieckmann, V., Horsfield, B., Schenk, H., 2000. Heating rate dependency of petroleum-forming reactions: implications for compositional kinetic predictions. Org. Geochem. 31, 1333–1348.

Dietrich, Andrew B., 2015. The Impact of Organic Matter on Geomechanical Properties and Elastic Anisotropy in the Vaca Muerta Shale. PhD diss. Colorado School of Mines. Arthur Lakes Library.

Eliyahu, Moshe, Emmanuel, Simon, Day-Stirrat, Ruarri J., Macaulay, Calum I., 2015. Mechanical properties of organic matter in shales mapped at the nanometer scale. Mar. Pet. Geol. 59, 294–304.

Espitalie, J., Deroo, G., Marquis, F., 1985. La pyrolyse Rock-Eval et ses applications. Deuxième partie. Revue de l'Institut français du Pétrole 40, 755–784.

Ferralis, Nicola, Matys, Emily D., Knoll, Andrew H., Hallmann, Christian, Summons, Roger E., 2016. Rapid, direct and non-destructive assessment of fossil organic matter via microRaman spectroscopy. Carbon 108, 440–449.

Ferrari, A.C., Robertson, J., 2000. Interpretation of Raman spectra of disordered and amorphous carbon. Phys. Rev. B 61, 14095.

Garcette-Lepecq, A., Derenne, S., Largeau, C., Bouloubassi, I., Saliot, A., 2000. Origin and formation pathways of kerogen-like organic matter in recent sediments off the Danube delta (northwestern Black Sea). Org. Geochem. 31, 1663–1683.

Guedes, A., Valentim, B., Prieto, A., Noronha, F., 2012. Raman spectroscopy of coal macerals and fluidized bed char morphotypes. Fuel 97, 443–449.

Hackley, P.C., 2012. Geological and geochemical characterization of the lower cretaceous Pearsall formation, Maverick Basin, South Texas: a future shale gas resource? AAPG Bull. 96, 1449–1482.

Hackley, P.C., Cardott, B.J., 2016. Application of organic petrography in north American shale petroleum systems: a review. Int. J. Coal Geol. 163, 8–51.

Hackley, P.C., Araujo, C.V., Borrego, A.G., Bouzinos, A., Cardott, B.J., Cook, A.C., Eble, C., Flores, D., Gentzis, T., Gonçalves, P.A., 2015. Standardization of reflectance measurements in dispersed organic matter: results of an exercise to improve interlaboratory agreement. Mar. Pet. Geol. 59, 22–34.

Hao, F., Zou, H., Gong, Z., Yang, S., Zeng, Z., 2007. Hierarchies of overpressure retardation of organic matter maturation: Case studies from petroleum basins in China. AAPG Bull. 91, 1467–1498.

Hicks, Stephanie C., Irizarry, Rafael A., 2018. A guide to teaching data science. Am. Stat. 72 (4), 382–391.

Hu, M., Cheng, Z., Zhang, M., Liu, M., Song, L., Zhang, Y., Li, J., 2014. Effect of calcite, kaolinite, gypsum, and montmorillonite on Huadian oil shale kerogen pyrolysis. Energy Fuel 28, 1860–1867.

Jacob, H., 1989. Classification, structure, genesis and practical importance of natural solid oil bitumen ("migrabitumen"). Int. J. Coal Geol. 11, 65–79.

Jarvie, D.M., Claxton, B.L., Henk, F., Breyer, J.T., 2001. Oil and Shale Gas from the Barnett Shale, Ft, Worth Basin, Texas (abs.): AAPG Annual Meeting Program. pp. A100.

Jehlička, Jan, Urban, Ondřej, Pokorný, Jan, 2003. Raman spectroscopy of carbon and solid bitumens in sedimentary and metamorphic rocks. Spectrochim. Acta A Mol. Biomol. Spectrosc. 59 (10), 2341–2352.

Jubb, Aaron M., Botterell, Palma J., Birdwell, Justin E., Burruss, Robert C., Hackley, Paul C., Valentine, Brett J., Hatcherian, Javin J., Wilson, Stephen A., 2018. High microscale variability in Raman thermal maturity estimates from shale organic matter. Int. J. Coal Geol. 199, 1–9.

Kadoura, A., Nair, A.K.N., Sun, S., 2016. Adsorption of carbon dioxide, methane, and their mixture by montmorillonite in the presence of water. Microporous Mesoporous Mater. 225, 331–341.

Kelemen, S., Fang, H., 2001. Maturity trends in Raman spectra from kerogen and coal. Energy Fuel 15, 653–658.

Khatibi, S., Aghajanpour, A., Ostadhassan, M., Ghanbari, E., Amirian, E., Mohammed, R., 2018a. Evaluating the Impact of Mechanical Properties of Kerogen on Hydraulic Fracturing of Organic Rich Formations, SPE Canada Unconventional Resources Conference. Society of Petroleum Engineers.

Khatibi, S., Ostadhassan, M., Aghajanpour, A., 2018b. Raman spectroscopy: an analytical tool for evaluating organic matter. J. Oil Gas Petrochem. Sci. 2, 00007.

Khatibi, S., Ostadhassan, M., Tuschel, D., Gentzis, T., Bubach, B., Carvajal-Ortiz, H., 2018c. Raman spectroscopy to study thermal maturity and elastic modulus of kerogen. Int. J. Coal Geol. 185, 103–118.

Khatibi, Seyedalireza, Ostadhassan, Mehdi, Tuschel, David, Gentzis, Thomas, Carvajal-Ortiz, Humberto, 2018d. Evaluating molecular evolution of kerogen by Raman spectroscopy: correlation with optical microscopy and Rock-Eval pyrolysis. Energies 11 (6), 1–19.

Killops, S.D., Killops, V.J., 2013. Introduction to Organic Geochemistry. John Wiley & Sons.

Klentzman, J.L., 2009. Geochemical Controls on Production in the Barnett Shale, Fort Worth Basin.

Kong, L., Ostadhassan, M.O., Sarout, J., Ling, K., Li, C., Wang, H., 2018. Impact of thermal maturation on wave velocity in the Bakken Shale. In: SPE Western Regional Meeting. Society of Petroleum Engineers.

Lawson, John, Erjavec, John, 2000. Modern Statistics for Engineering and Quality Improvement. Duxbury Press.

LeFever, Julie A., Le Fever, Richard D., Nordeng, Stephan H., 2011. Revised Nomenclature for the Bakken Formation (Mississippian-Devonian), North Dakota. pp. 11–26.

Lewan, M., 1993. Laboratory Simulation of Petroleum Formation, Organic Geochemistry. Springer, pp. 419–442.

Lewan, M., 1997. Experiments on the role of water in petroleum formation. Geochim. Cosmochim. Acta 61, 3691–3723.

Lewan, M.D., Roy, S., 2011. Role of water in hydrocarbon generation from Type-I kerogen in Mahogany oil shale of the Green River Formation. Org. Geochem. 42, 31–41.

Lewan, M., Ruble, T., 2002. Comparison of petroleum generation kinetics by isothermal hydrous and nonisothermal open-system pyrolysis. Org. Geochem. 33, 1457–1475.

Lewan, M., Winters, J., McDonald, J., 1979. Generation of oil-like pyrolyzates from organic-rich shales. Science 203, 897–899.

Li, Chunxiao, Ostadhassan, Mehdi, Gentzis, Thomas, Kong, Lingyun, Carvajal-Ortiz, Humberto, Bubach, Bailey, 2018a. Nanomechanical characterization of organic matter in the Bakken formation by microscopy-based method. Mar. Pet. Geol. 96, 128–138.

Li, Chunxiao, Ostadhassan, Mehdi, Guo, Senli, Gentzis, Thomas, Kong, Lingyun, 2018b. Application of PeakForce tapping mode of atomic force microscope to characterize nanomechanical properties of organic matter of the Bakken Shale. Fuel 233, 894–910.

Li, Huijun, Wu, Tairan, Ma, Zongjin, Zhang, Wencai, 2004. Pressure retardation of organic maturation in clastic reservoirs: a case study from the Banqiao Sag, Eastern China. Marine and Petroleum Geology 21 (9), 1083–1093.

Liang, M., Wang, Z., Zheng, J., Li, X., Wang, X., Gao, Z., Luo, H., Li, Z., Qian, Y., 2015. Hydrous pyrolysis of different kerogen types of source rock at high temperature-bulk results and biomarkers. J. Pet. Sci. Eng. 125, 209–217.

Liu, DeHan, Xiao, XianMing, Tian, Hui, Min, YuShun, Zhou, Qin, Cheng, Peng, Shen, JiaGui, 2013. Sample maturation calculated using Raman spectroscopic parameters for solid organics: methodology and geological applications. Chin. Sci. Bull. 58 (11), 1285–1298.

Liu, Kouqi, Ostadhassan, Mehdi, Kong, Lingyun, 2017. Pore structure heterogeneity in middle Bakken formation. In: 51st US Rock Mechanics/Geomechanics Symposium. American Rock Mechanics Association.

Liu, Yuke, Xiong, Yongqiang, Li, Yun, Peng, Pingan, 2018. Effect of thermal maturation on chemical structure and nanomechanical properties of solid bitumen. Marine and Petroleum Geology 92, 780–793.

Lünsdorf, N.K., 2016. Raman spectroscopy of dispersed vitrinite—methodical aspects and correlation with reflectance. Int. J. Coal Geol. 153, 75–86.

Lupoi, Jason S., Fritz, Luke P., Parris, Thomas M., Hackley, Paul C., Solotky, Logan, Eble, Cortland F., Schlaegle, Steve, 2017. Assessment of thermal maturity trends in Devonian–Mississippian source rocks using raman spectroscopy: limitations of Peak-Fitting method. Front. Energy Res. 5, 24.

Mackenzie, A., McKenzie, D., 1983. Isomerization and aromatization of hydrocarbons in sedimentary basins formed by extension. Geol. Mag. 120, 417–470.

Mansuy, L., Landais, P., Ruau, O., 1995. Importance of the reacting medium in artificial maturation of a coal by confined pyrolysis. 1. Hydrocarbons and polar compounds.

Energy Fuel 9, 691–703.
McTavish, R., 1998. The role of overpressure in the retardation of organic matter maturation. J. Pet. Geol. 21, 153–186.
Michels, R., Landais, P., 1994. Artificial coalification: comparison of confined pyrolysis and hydrous pyrolysis. Fuel 73, 1691–1696.
Michels, R., Landais, P., Torkelson, B., Philp, R., 1995. Effects of effluents and water pressure on oil generation during confined pyrolysis and high-pressure hydrous pyrolysis. Geochim. Cosmochim. Acta 59, 1589–1604.
Monthioux, M., 1988. Expected mechanisms in nature and in confined-system pyrolysis. Fuel 67, 843–847.
Monthioux, M., Landais, P., 1987. Evidence of free but trapped hydrocarbons in coals. Fuel 66, 1703–1708.
Monthioux, M., Landais, P., Monin, J.-C., 1985. Comparison between natural and artificial maturation series of humic coals from the Mahakam delta, Indonesia. Org. Geochem. 8, 275–292.
Mumm, Andreas Schmidt, İnan, Sedat, 2016. Microscale organic maturity determination of graptolites using Raman spectroscopy. Int. J. Coal Geol. 162, 96–107.
Myers, G.A., Kehoe, K., Hackley, P., 2017. Analysis of Artificially Matured Shales With Confocal Laser Scanning Raman Microscopy: Applications to Organic Matter Characterization. Unconventional Resources Technology Conference (URTEC).
Olson, R.K., 2008. Cutting Analyses, in Coalbed Methane and Shale Gas Exploration Strategies: Workshop for Sorbed Gas Reservoir Systems: AAPG Course 15, AAPG Annual Convention, San Antonio, Texas. April 24–25, 2008. pp. 35.
Ostadhassan, M., Liu, K., Li, C., Khatibi, S., 2018. Geochemical Properties, Fine Scale Characterization of Shale Reservoirs. Springer, pp. 57–70.
Pan, C., Geng, A., Zhong, N., Liu, J., Yu, L., 2009. Kerogen pyrolysis in the presence and absence of water and minerals: amounts and compositions of bitumen and liquid hydrocarbons. Fuel 88, 909–919.
Pan, C., Jiang, L., Liu, J., Zhang, S., Zhu, G., 2010. The effects of calcite and montmorillonite on oil cracking in confined pyrolysis experiments. Org. Geochem. 41, 611–626.
Petersen, H.I., Schovsbo, N.H., Nielsen, A.T., 2013. Reflectance measurements of zooclasts and solid bitumen in lower Paleozoic shales, southern Scandinavia: correlation to vitrinite reflectance. Int. J. Coal Geol. 114, 1–18.
Piani, L., Robert, F., Beyssac, O., Binet, L., BOUROT-DENISE, M., Derenne, S., Le Guillou, C., Marrocchi, Y., Mostefaoui, S., ROUZAUD, J.N., 2012. Structure, composition, and location of organic matter in the enstatite chondrite Sahara 97096 (EH3). Meteorit. Planet. Sci. 47, 8–29.
Potgieter-Vermaak, S., Maledi, N., Wagner, N., Van Heerden, J.H.P., Van Grieken, R., Potgieter, J.H., 2011. Raman spectroscopy for the analysis of coal: a review. J. Raman Spectrosc. 42 (2), 123–129.
Quirico, E., Rouzaud, J.-N., Bonal, L., Montagnac, G., 2005. Maturation grade of coals as revealed by Raman spectroscopy: progress and problems. Spectrochim. Acta A Mol. Biomol. Spectrosc. 61, 2368–2377.
Riediger, C., 1993. Solid bitumen reflectance and Rock-Eval Tmax as maturation indices: an example from the "Nordegg Member", Western Canada Sedimentary Basin. Int. J. Coal Geol. 22, 295–315.
Rullkötter, J., Marzi, R., 1988. Natural and artificial maturation of biological markers in a Toarcian shale from northern Germany. Org. Geochem. 13, 639–645.
Sadezky, Alexa, Muckenhuber, Harald, Grothe, Hinrich, Niessner, R., Pöschl, Ulrich, 2005. Raman microspectroscopy of soot and related carbonaceous materials: spectral analysis and structural information. Carbon 43 (8), 1731–1742.
Sauerer, B., Craddock, P.R., AlJohani, M.D., Alsamadony, K.L., Abdallah, W., 2017. Fast and accurate shale maturity determination by Raman spectroscopy measurement with minimal sample preparation. Int. J. Coal Geol. 173, 150–157.
Schito, A., Romano, C., Corrado, S., Grigo, D., Poe, B., 2017. Diagenetic thermal evolution of organic matter by Raman spectroscopy. Org. Geochem. 106, 57–67.
Schmidt, J.S., Hinrichs, R., Araujo, C.V., 2017. Maturity estimation of phytoclasts in strew mounts by micro-Raman spectroscopy. Int. J. Coal Geol. 173, 1–8.
Schrader, B., 2008. Infrared and Raman Spectroscopy: Methods and Applications. John Wiley & Sons.
Schumacher, M., Christl, I., Scheinost, A.C., Jacobsen, C., Kretzschmar, R., 2005. Chemical heterogeneity of organic soil colloids investigated by scanning transmission X-ray microscopy and C-1s NEXAFS microspectroscopy. Environ. Sci. Technol. 39, 9094–9100.
Spötl, C., Houseknecht, D.W., Jaques, R.C., 1998. Kerogen maturation and incipient graphitization of hydrocarbon source rocks in the Arkoma Basin, Oklahoma and Arkansas: a combined petrographic and Raman spectrometric study. Org. Geochem. 28, 535–542.
Steptoe, Anne, 2012. Petrofacies and depositional systems of the Bakken Formation in the Williston Basin, North Dakota. Masters Abstracts Int., vol. 51 (03).
Tegelaar, E.W., Noble, R.A., 1994. Kinetics of hydrocarbon generation as a function of the molecular structure of kerogen as revealed by pyrolysis-gas chromatography. Org. Geochem. 22, 543–574.
Tian, H., Xiao, X., Wilkins, R., Li, X., Gan, H., 2007. Gas sources of the YN2 gas pool in the Tarim Basin—evidence from gas generation and methane carbon isotope fractionation kinetics of source rocks and crude oils. Mar. Pet. Geol. 24, 29–41.
Tissot, B.P., Welte, D.H., 1984. Diagenesis, catagenesis and metagenesis of organic matter. In: Petroleum Formation and Occurrence. Springer, pp. 69–73.
Tuinstra, F., Koenig, J. Lo, 1970. Raman spectrum of graphite. J. Chem. Phys. 53 (3), 1126–1130.
Tyson, R.V., 1995. Abundance of organic matter in sediments: TOC, hydrodynamic equivalence, dilution and flux effects. In: Sedimentary Organic Matter. Springer, pp. 81–118.
Valentine, B.J., Hackley, P.C., Enomoto, C.B., Bove, A.M., Dulong, F.T., Lohr, C.D., Scott, K.R., 2014. Organic petrology of the Aptian-age section in the downdip Mississippi Interior Salt Basin, Mississippi, USA: Observations and preliminary implications for thermal maturation history. Int. J. Coal Geol. 131, 378–391.
Van Krevelen, D.W., 1993. Coal: Typology, Physics, Chemistry, Constitution. Elsevier Amsterdam.
Waples, Douglas Wendle, 1981. Organic Geochemistry for Exploration Geologists. Burgess Pub. Co.
Wu, L.M., Zhou, C.H., Keeling, J., Tong, D.S., Yu, W.H., 2012. Towards an understanding of the role of clay minerals in crude oil formation, migration and accumulation. Earth Sci. Rev. 115, 373–386.
Yang, Chin-Shung, Kao, Szu-Pyng, Lee, Fen-Bin, Hung, Pen-Shan, 2004. Twelve different interpolation methods: A case study of Surfer 8.0. In: Proceedings of the XXth ISPRS Congress. vol. 35. pp. 778–785.
Yang, J., Hatcherian, J., Hackley, P.C., Pomerantz, A.E., 2017. Nanoscale geochemical and geomechanical characterization of organic matter in shale. Nat. Commun. 8, 2179.
Zargari, Saeed, 2015. Effect of Thermal Maturity on Nanomechanical Properties and Porosity in Organic Rich Shales (a Bakken Shale Case Study). PhD diss. Colorado School of Mines. Arthur Lakes Library.
Zhang, Liya, Buatois, Luis A., 2016. Sedimentology, ichnology and sequence stratigraphy of the Upper Devonian–lower Mississippian Bakken Formation in eastern Saskatchewan. Bull. Can. Petrol. Geol. 64 (3), 415–437.
Zhou, Q., Xiao, X., Pan, L., Tian, H., 2014. The relationship between micro-Raman spectral parameters and reflectance of solid bitumen. Int. J. Coal Geol. 121, 19–25.
Zhu, G., Zhang, S., Su, J., Zhang, B., Yang, H., Zhu, Y., Gu, L., 2013. Alteration and multistage accumulation of oil and gas in the Ordovician of the Tabei Uplift, Tarim Basin, NW China: implications for genetic origin of the diverse hydrocarbons. Mar. Pet. Geol. 46, 234–250.